

# STELLAR LOCUS REGRESSION: ACCURATE COLOR CALIBRATION, AND THE REAL-TIME DETERMINATION OF GALAXY CLUSTER PHOTOMETRIC REDSHIFTS

F. WILLIAM HIGH, CHRISTOPHER W. STUBBS, ARMIN REST, BRIAN STALDER, PETER CHALLIS

Department of Physics

and

Harvard-Smithsonian Center for Astrophysics

Harvard University and

Cambridge, MA

*Draft version October 27, 2018*

## ABSTRACT

We present Stellar Locus Regression (SLR), a method of directly adjusting the instrumental broadband optical colors of stars to bring them into accord with a universal stellar color-color locus, producing accurately calibrated colors for both stars and galaxies. This is achieved without first establishing individual zeropoints for each passband, and can be performed in real-time at the telescope. We demonstrate how SLR naturally makes one wholesale correction for differences in instrumental response, for atmospheric transparency, for atmospheric extinction, and for Galactic extinction. We perform an example SLR treatment of SDSS data over a wide range of Galactic dust values and independently recover the direction and magnitude of the canonical Galactic reddening vector with 14–18 mmag RMS uncertainties. We then isolate the effect of atmospheric extinction, showing that SLR accounts for this and returns precise colors over a wide of airmass, with 5–14 mmag RMS residuals. We demonstrate that SLR-corrected colors are sufficiently accurate to allow photometric redshift estimates for galaxy clusters (using red sequence galaxies) with an uncertainty  $\sigma(z)/(1+z) = 0.6\%$  per cluster for redshifts  $0.09 < z < 0.25$ . Finally, we identify our objects in the 2MASS all-sky catalog, and produce *i*-band zeropoints typically accurate to 18 mmag using only SLR. We offer open-source access to our IDL routines, validated and verified for the implementation of this technique, at <http://stellar-locus-regression.googlecode.com>.

*Subject headings:* galaxies: fundamental parameters — methods: data analysis — stars: fundamental parameters — stars: statistics — techniques: photometric

## 1. INTRODUCTION

The observed broadband colors—*i.e.* flux ratios—of celestial objects depend on the photon spectral energy distribution of the source; on extragalactic, Galactic and atmospheric scattering and absorption along the line of sight; and on the instrumental sensitivity function over the wavelengths of interest. One challenge of astronomical photometric analysis is to disentangle, from a given set of observations, the source’s colors from such a plethora of perturbing factors.

Colors hold information about a source’s type, temperature, metallicity, and redshift. A source’s apparent magnitude, on the other hand, also depends on its distance and on the size and nature of the emitting regions. We assert that for almost all astrophysical endeavors, accurate photometric *colors* are more useful than high accuracy *magnitudes*, especially because we seldom know distances well enough to convert from apparent to absolute magnitudes at the percent level. Furthermore, for photometric redshift techniques that use a prior on magnitudes, the broad luminosity function of galaxies generates a span in magnitude that far exceeds the range in color, for a given galaxy type at a particular redshift.

The current and next generation of wide-field multicolor survey projects include the CFHTLS<sup>1</sup>,

PanSTARRS<sup>2</sup>, BCS<sup>3</sup>, DES<sup>4</sup>, LSST<sup>5</sup>, and SkyMapper<sup>6</sup>. Object classification and distance estimation with photometric redshifts are necessary starting points for extragalactic science using these surveys, and these in turn depend on knowing calibrated colors. The technique we describe here can be used very early in a survey to obtain highly accurate colors of objects, as well as magnitude estimates. This should allow more rapid exploitation of new survey data—indeed, of nearly any multiband data.

The standard approach to determining colors of sources is to first calibrate magnitudes in all observed passbands (such as *g*, *r*, *i*, and *z*), and then subtract the calibrated magnitudes to obtain calibrated colors (*g* – *r*, *g* – *i*, *etc.*). This is typically time-consuming, both at the telescope and in the analysis phase. Establishing photometric zeropoints for a stack of multiband images requires separate observations of spectrophotometric standard stars to measure the instrumental sensitivity and estimate atmospheric extinction, and spatiotemporal interpolation of the calibration parameters to the science fields under “photometric conditions.”

In this paper we describe how to calibrate colors directly from objects cataloged from multiband, flat-fielded images of a field, without having to first determine the

<sup>2</sup> <http://pan-starrs.ifa.hawaii.edu/public/>

<sup>3</sup> <http://cosmology.uiuc.edu/BCS/>

<sup>4</sup> <https://www.darkenergysurvey.org/>

<sup>5</sup> [http://www.lsst.org/Science/lsst\\_baseline.shtml](http://www.lsst.org/Science/lsst_baseline.shtml)

<sup>6</sup> <http://msowww.anu.edu.au/skymapper/>

Electronic address: [high@physics.harvard.edu](mailto:high@physics.harvard.edu)

<sup>1</sup> <http://www.cfht.hawaii.edu/Science/CFHTLS/>

corresponding photometric zeropoints, and without the usual repeated measurements of standard stars. We demonstrate how this can be done accurately, yielding colors accurate to a few percent, and rapidly, allowing for optimal use of allocated telescope time.

Our technique exploits the optical and infrared color-color *stellar locus* (cf. Covey et al. 2007; Ivezić et al. 2007), the one-dimensional and astrophysically fundamental track that stars occupy in color-color space. The majority of stars lie somewhere along this locus, at a position that depends primarily upon effective temperature. The universality of the stellar locus was exploited in the Oxford-Dartmouth Thirty-Degree Survey (“stellar locus fitting,” MacDonald et al. 2004) to stabilize photometric zeropoints in non-photometric conditions, and in Sloan Digital Sky Survey’s (SDSS) Stripe 82 (“stellar locus method,” Ivezić et al. 2007) to account for differences in the response function of different detectors in the SDSS instrument. Our approach is different from these mainly because we do not first establish photometric zeropoints per band: we immediately calibrate colors in all fields, and only optionally solve for the calibrated apparent magnitudes, using the stellar locus. We do not use SLR as a diagnostic or corrective tool, but as our primary calibrator.

Our Stellar Locus Regression (SLR) approach builds on these previous pioneering works. We establish the location of the stellar feature in instrumental color-color space, and we determine what transformations are needed to bring this into coincidence with the known location of a standard stellar locus. Applying appropriate color-corrections to the entire rest of the catalog automatically accounts for all of the standard calibration terms, including zeropoints, atmospheric extinction, aperture corrections, and Galactic extinction. The technique is straightforward, fast, and allows observers to forgo the usual standard star observations altogether because all observed stars are expected to lie along the same stellar locus. We have calibrated fields with SLR using as few as 7 stars in fields of view as small as  $4' \times 8'$ .

Figure 1 schematically illustrates the technique. We perform SLR on new data (see §4.2-4.4) taken with the IMACS instrument (Dressler et al. 2003; Osip et al. 2008) on the Magellan 6.5 m telescope. All panels show our adopted standard stellar locus line and stellar density contours, reproduced from Covey et al. (2007, §2.1), along with 36 IMACS stellar colors (red points). The top panels show instrumental stellar colors with the standard locus. We perform SLR, neglecting instrumental color terms, with results shown in the middle panels. We perform SLR again after measuring color terms independently from an external standard star field, with results shown in the bottom panels. By way of illustration, the vectors in the middle panels show the expected direction and magnitude of extinction by Galactic dust ( $A_r = 0.2$  mag and  $R_V = 3.1$ , estimated using Schlegel et al. 1998) and the atmosphere (1.3 airmasses).

We adopt a standard stellar locus in §2, and then motivate and build a picture of what comprises it so as to understand its universality. In §3 we outline the mathematics of color calibration and describe an optimal algorithm for real-time color calibration, which we apply to real data in a series of tests (§4). In §4.1 we perform our first test, applying SLR to already-calibrated

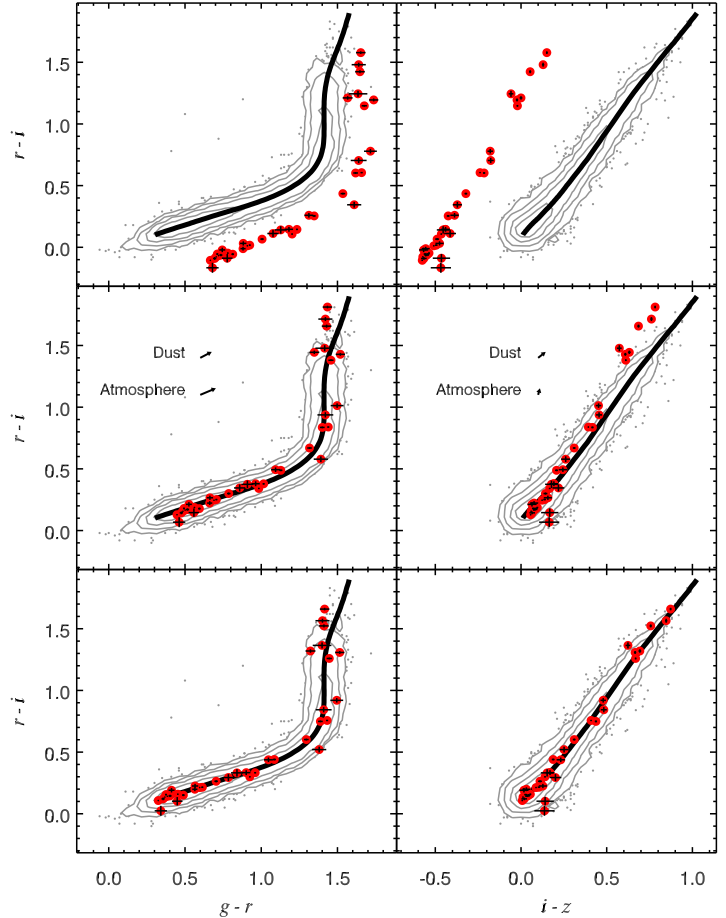


FIG. 1.— An illustration of Stellar Locus Regression (SLR). Colors are plotted on the SDSS photometric system. All panels show the standard stellar locus (black line and gray density contours), reproduced from Covey et al. (2007). Red points are stellar colors obtained from a Source Extractor analysis of flat-fielded Magellan 6.5 m IMACS images. *Top panels*: The instrumental IMACS colors are plotted, with a clear mismatch between them and the standard locus. *Middle panels*: SLR is performed with only a common translation vector applied to the instrumental colors. Note the color-dependent discrepancies in the upper right portions of the central panels. By way of example, the vectors show the expected direction and magnitude of extinction by Galactic dust ( $A_r = 0.2$ ) and the atmosphere (1.3 airmasses). *Bottom panels*: Color terms are measured from a single observation of a field containing standard stars. Fixing these color terms, a new best-fit translation is determined, which brings the observed colors onto the SDSS-calibrated color system, as defined by the stellar locus. This SLR analysis, when the corrections are then applied to all objects in the photometric catalog, allows us to rapidly obtain highly accurate colors on the SDSS system, directly from flat-fielded data, with a single correction step that accounts for atmospheric extinction, Galactic extinction and instrumental response differences.

SDSS photometry, where we recover the canonical Galactic reddening vector in direction and magnitude over a wide range of dust thicknesses. Section 4.2 examines the fundamental repeatability of SLR color and magnitude measurements by comparing SDSS data to data from a different instrument. Section 4.3 isolates the effect of atmospheric extinction. Our final test appears in §4.4, where we recover the spectroscopic redshifts of 11 low redshift galaxy clusters to high accuracy using only SLR colors. We end with a discussion (§5) and conclusions (§6).

The nearly-blackbody emission spectra of stars place them predominantly along a line in optical and infrared color-color space. Stellar color therefore depends primarily on effective temperature and is the basis for the Morgan-Keenan (MK) stellar classification system (Morgan et al. 1943). Real stellar atmospheres deviate from blackbody behavior because of molecular absorption and metallicity effects. Observations, which capture stellar light that has traversed the dust of our galaxy, our atmosphere, and our telescope systems, will produce stellar color loci that deviate further from the expected intrinsic behavior. We have based our SLR approach on the assumption that we can identify a stellar locus in *grizJHK* color space that is intrinsically universal. We explore the extent to which this is true by inspecting what comprises an observed stellar locus.

### 2.1. A Standard Locus

We adopt as our standard the empirical stellar locus of Covey et al. (2007). Those authors calculated the running-median of the colors of  $\sim 10^5$  stars, from high quality observations by both the SDSS and 2MASS surveys. The line-of-sight Galactic dust for their sample was estimated from the maps of Schlegel et al. (1998, SFD) to be  $A_r < 0.2$ . We additionally smooth this locus line with a 0.2 mag size boxcar averaging kernel to reduce some of the scatter between adjacent points. These are the data we present in Figure 1—we call this the standard stellar locus line.

The two most salient features of the standard locus are its nearly one-dimensional nature and a dramatic break or kink in the  $(g-r, r-i)$  plane at  $r-i \sim 0.7$ . As we explore below (§2.2), blue-ward of the kink are mainly evolved and main sequence (MS) A- through K-type stars, and red-ward are mainly M-type dwarfs (Finlator et al. 2000; Hawley et al. 2002; Covey et al. 2007; Jurić et al. 2008).

Because of the well-defined relationships between the color (effective temperature), age, and intrinsic luminosity of stars, each point along the stellar locus probes roughly predictable 3-dimensional spatial volumes, given some fixed dynamic range for the observations. The reddest MS stars that make up the  $r-i > 0.7$  branch of the stellar locus are less luminous, so the effective volume an observation probes is small and nearby. Likewise, bluer MS and evolved stars are intrinsically brighter, so the effective volumes probed at those colors are larger and farther away—and because both MS and evolved stars constitute the  $r-i < 0.7$  portion of the stellar locus, observations are sensitive to a plurality of volumes and distances.

A comprehensive Galactic structure and population synthesis analysis is beyond the scope of this paper, but we will explore below the factors that give rise to uniformity in the *observed* stellar locus, including the dramatic color-volume effects at typical SDSS depths.

### 2.2. Color-Volume Effects

Each pointing of an astronomical camera images a cone-shaped region of space, set by the solid-angle field of view  $\Omega$  of the instrument. For a single frame there is also a limited observable dynamic range in apparent magnitude: the brightest observable objects are determined

TABLE 1  
DETECTABILITY VOLUMES VS. ABSOLUTE MAGNITUDE.

$M_r$ <sup>a</sup> (AB mag)	$R_{\text{inner}}$ <sup>b</sup> (pc)	$R_{\text{outer}}$ <sup>c</sup> (pc)	Detectability Volume <sup>d</sup> (arb units)
-5	6.3E4	2.5E6	1.0E12
-4	4.0E4	1.6E6	2.8E11
-3	2.5E4	1.0E6	6.3E10
-2	1.6E4	6.3E5	1.6E10
-1	1.0E4	4.0E5	4.0E9
0	6.3E3	2.5E5	1.0E9
1	4.0E3	1.6E5	2.5E8
2	2.5E3	1.0E5	6.3E7
3	1.6E3	6.3E4	1.6E7
4	1.0E3	4.0E4	4.0E6
5	6.3E2	2.5E4	1.0E6
6	4.0E2	1.6E4	2.5E5
7	2.5E2	1.0E4	6.3E4
8	1.6E2	6.3E3	1.6E4
9	1.0E2	4.0E3	4.0E3
10	6.3E1	2.5E3	1.0E3
11	4.0E1	1.6E3	2.5E2
12	2.5E1	1.0E3	6.3E1
13	1.6E1	6.3E2	1.6E1
14	1.0E1	4.0E2	4.0E0
15	6.3E0	2.5E2	1.0E0

<sup>a</sup> Absolute magnitudes of stars in the SDSS  $r$ -band.

<sup>b</sup> Closest distances (in parsecs) for the object to be observable, for a notional saturation limit of  $r = 14$ .

<sup>c</sup> Furthest distances (in parsecs) for a  $10\sigma$  detection limit of  $r = 22$ .

<sup>d</sup> Volume (in arbitrary units) within which objects of a given absolute magnitude can be detected, subject to the instrumental dynamic range constraints.

by the saturation limit of the system, and the faintest useful objects must satisfy some selection in signal-to-noise ratio. A star of a particular absolute magnitude and corresponding color is therefore detectable within a truncated cone of opening angle  $\Omega$ , with an near-edge determined by the saturation limit and a far-edge set by the required signal-to-noise ratio. For simplicity we assume an unextincted line of sight.

Table 1 illustrates the dramatic selection-effect of dynamic range on observed stars of various intrinsic luminosities. We take a notional saturation limit of  $r = 14$  and a faint detection limit at  $r = 22$ , which are approximate values appropriate for SDSS. For a dynamic range of 8 mag, the outer detection edge of the detectability cone is always  $\sim 39$  times farther away than its inner saturation edge, for a given absolute magnitude object. Table 1 also shows that for each additional magnitude increase of stellar luminosity, the survey volume increases by a factor of four. Luminous stars are detectable over a vastly larger volume than fainter stars, since the outer edge of the detectability region is *proportional* to the distance to the inner edge.

As a concrete example, at SDSS depths and Galactic latitudes  $|b| = 90$  deg, absolute magnitudes  $M_r \gtrsim 12$  are detectable only closer than  $\sim 1$  kpc, which is the height of the Galactic disk (Jurić et al. 2008). Objects with  $M_r \lesssim 4$  are seen only at Galactic heights  $|Z| > 1$  kpc, so are in the halo.

Absolute stellar magnitude varies with stellar color and age in well understood ways. To explore the relation in the SDSS magnitude system, we used the model stellar populations of Marigo et al. (2008,

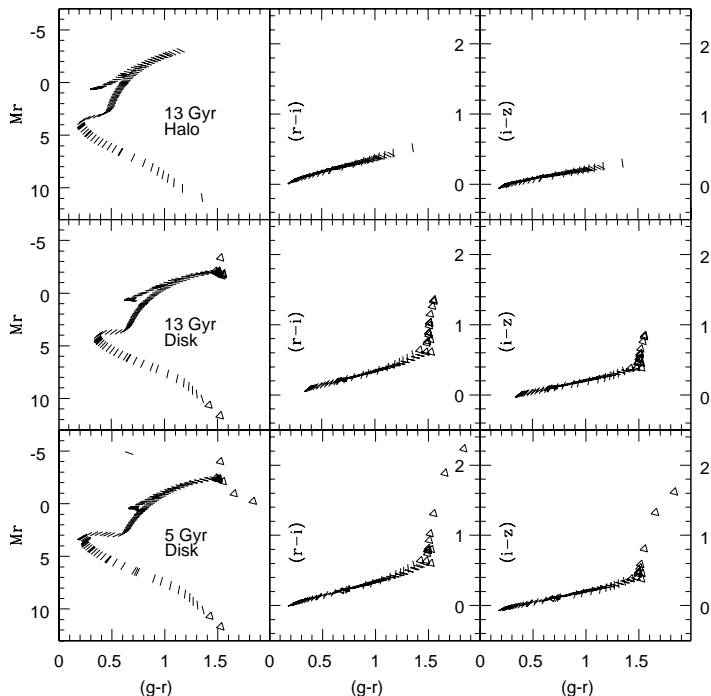


FIG. 2.— Comparisons of modeled  $M_r$  vs.  $g-r$  color-magnitude diagrams (left column),  $r-i$  vs.  $g-r$  (central column), and  $i-z$  vs.  $g-r$  (rightmost column) color-color diagrams for different stellar populations, for zero Galactic extinction. The upper row corresponds to a stellar halo population with  $[\text{Fe}/\text{H}] = -1.5$  and an age of 13 Gyrs. The central row also corresponds to a 13 Gyr age, but with a characteristic disk metallicity;  $[\text{Fe}/\text{H}] = -0.5$ . The bottom row is what one might expect for more recent star formation in the Galactic disk, with  $[\text{Fe}/\text{H}] = -0.5$  and an age of 5 Gyr. Absolute magnitudes are indicated by the *angle* of the whisker, with  $\theta = 9M_r \text{ mag}^{-1} \text{ deg}$ . Objects with  $r-i > 0.7$  are shown as triangles. Only stellar populations with  $[\text{Fe}/\text{H}] > -0.7$  produce the excursion to  $r-i > 0.7$ , seen in the central and lower rows, that is essential to the SLR method.

[http://stev.oapd.inaf.it/cgi-bin/cmd\\_2.1](http://stev.oapd.inaf.it/cgi-bin/cmd_2.1)). This online tool modeled stars with initial masses down to  $0.15 M_{\odot}$ . We have just shown that the typical SDSS dynamic range is sensitive to both halo and disk stars, so we consider three models, using Ivezić et al. (2008) as a guide:

1. a 13 Gyr halo population, with a metallicity  $[\text{Fe}/\text{H}]_{\text{halo}} = -1.5$ ,
2. a 13 Gyr disk population of higher metallicity,  $[\text{Fe}/\text{H}]_{\text{disk}} = -0.5$ , and
3. a 5 Gyr disk population of higher metallicity,  $[\text{Fe}/\text{H}]_{\text{disk}} = -0.5$ .

Figure 2 shows the color-magnitude and color-color diagrams that illustrate the connection between absolute magnitudes and regions in color-color space for these populations.

Figure 2 shows that only disk-metallicity stars populate the locus red-ward of the kink. The main sequence M dwarfs in this color range have  $M_r \gtrsim 11$  mag and so in the SDSS dynamic range these objects lie at distances  $\lesssim 1.5$  kpc from Earth. These stars are almost entirely in the disk. The M giants red-ward of the kink have

$M_r \lesssim -2$  mag corresponding to distances  $\gtrsim 15$  kpc. Few disk-metallicity stars lie at such distances (Ivezić et al. 2008). Therefore the vast majority of the stars that populate the  $(r-i) > 0.7$  region of the locus at SDSS depths are disk dwarfs. Hawley et al. (2002) also support this viewpoint, attributing SDSS objects with  $1 < (r-i) < 2$  to M0 through M6 stars at typical distances ranging from 1 to 0.1 kpc respectively.

Continuing these arguments, stellar locus stars blue-ward of the  $(r-i) \sim 0.7$  kink comprise of a blend of MS disk stars, MS halo stars, and evolved (post-turnoff) halo stars. The luminosity of the bluer MS stars are  $4 \text{ mag} \lesssim M_r \lesssim 11 \text{ mag}$  and are detectable from both the disk and halo. We also see that even for a stellar population 13 Gyrs old, with a main sequence turnoff at around  $M_r \sim 4$ , blue turnoff stars that are closer than 1 kpc would saturate the detector.

The relative proportion of disk and halo stars that make up the stellar locus at  $(r-i) < 0.7$  (blue-ward of the kink) is magnitude dependent. Ivezić et al. (2008) show that for  $0.2 < (g-r) < 0.4$ , at  $g \sim 17.5$  half the stars have metallicity characteristic of the disk, and half are halo stars. At fainter magnitudes the proportion of halo stars increases.

Armed with this understanding of the observed stellar locus's constituent populations, we explore the effect their corresponding metallicity distributions should have.

### 2.3. Metallicity

A number of previous authors have explored the influence of metallicity on stellar colors in the SDSS photometric system (Lenz et al. 1998; Covey et al. 2007; Jurić et al. 2008; Ivezić et al. 2008). Ivezić et al. (2008) demonstrated that most halo stars have a common metallicity that is reasonably well described by a Gaussian distribution with median  $[\text{Fe}/\text{H}]_{\text{halo}} = -1.5$  and width  $\sigma_{\text{halo}} = 0.3$  dex. The median disk metallicity was shown to be about  $-0.5$  and exhibits half the scatter of the halo, with  $\sigma_{\text{disk}} = 0.16$  dex.

The biggest observable broadband effect from metallicity occurs in the  $u$ -band, which is one of the reasons we exclude that band from consideration here. Stellar metallicity effects in  $g-r$  are ten times smaller than in  $u-g$ . Using this fact and Figure 21 of Ivezić et al. (2008), the expected spread in  $g-i$  color for halo stars should be of order 0.05 mag. This is a conservative upper limit estimate of the intrinsic width of the halo contribution to the stellar locus from metallicity alone.

We have modeled the effect of metallicity on the stellar MS, and present some of the results in Table 2. We used a grid of model atmospheres derived from the Phoenix project (Brott & Hauschildt 2005) and the Kurucz (1993) library for the typical disk and halo metallicities,  $[\text{Fe}/\text{H}] = -0.5$  and  $-1.5$  dex. The range of parameters used was  $3,500\text{K} \leq T_{\text{eff}} \leq 10,000\text{K}$  for M5 to A0 using the Phoenix models and  $15,000\text{K} \leq T_{\text{eff}} \leq 45,000\text{K}$  for B5 to O5 from the Kurucz (1993) models, and we adopted a typical main sequence  $\log(g)$  for each spectral type. We then calculated the broadband colors based on the SDSS filter and CCD throughput.

We found that the greatest influence of metallicity on broadband color is in the late-type stars (around M0 and later) and is in opposite direction to the color displacement of early-type stars. The relatively cool atmospheres

TABLE 2  
MODEL STELLAR COLOR DIFFERENCE  
BETWEEN  $Z=-0.5$  AND  $Z=-1.5$ .

MK type	$\delta(g-r)^a$	$\delta(r-i)^a$	$\delta(i-z)^a$
O5V	-0.005	-0.002	-0.003
B0V	-0.000	-0.002	-0.002
B5V	-0.003	-0.002	-0.005
A0V	-0.000	-0.004	-0.003
A5V	0.004	-0.007	-0.007
F0V	0.004	-0.010	-0.012
F5V	0.019	-0.009	-0.013
G0V	0.031	-0.012	-0.015
G5V	0.037	-0.013	-0.015
K0V	0.053	-0.015	-0.014
K5V	0.124	0.002	-0.014
M0V	0.004	0.067	0.031
M5V	-0.137	0.117	0.080

<sup>a</sup> As a comparison, for galactic extinction ( $A_r = 0.2$ ) the color perturbation is (0.076, 0.048, 0.044); for 1.3 atmospheres of extinction, the color perturbation is (0.103, 0.053, 0.010).

of the red stars are rich with molecules, and the molecular absorption features blend together with other lines to form a continuum that differs substantially from a blackbody spectrum. We also observed that a minimum metallicity of  $[\text{Fe}/\text{H}] = -0.7$  is needed for red stars to populate the locus red-ward of the kink. Less metallicity “irons out” the kink, making the model colors colinear with the bluer stars. This observation is consistent with the conclusions drawn in §2.2. A continuum of metallicities near this threshold would smear the observed stellar locus in the redder region. The apparent lack of such smearing in the observed locus indicates the paucity of stars at this intermediate metallicity, as found by Ivezić et al. (2008). It is therefore the high mean metallicity and molecular absorption of disk stars that produce the kink in the SDSS stellar locus in the first place, and that make our implementation of SLR possible.

#### 2.4. Age

Younger stellar populations have a brighter, bluer main sequence turnoff point, and this shifts the blue tip of the stellar locus towards the blue. This does not distort the basic shape of the stellar locus. For very young populations at high metallicity there is also a red-ward extension of the main locus, due to massive stars evolving to  $r-i > 0.7$ , but we concluded in §2.2 that these stars do not appear in the stellar locus at SDSS depths, since these young stars would be in the disk and would saturate. Other features in the color-magnitude diagram, such as helium-burning loops, essentially remain confined to the standard locus line and do not change its shape. Our methods (§3) are therefore expected to be largely insensitive to population age effects.

#### 2.5. Binaries and Unresolved Superpositions

Superpositions of stars, either as physical binaries or chance coincidences, most often fall within the standard locus area, but can also produce systematic outliers and therefore change the observed stellar locus shape. For the latter to happen, the objects within a single PSF

must have different colors, but similar magnitudes. One can adopt two philosophical resolutions to this issue.

One approach is to realize that both our standard locus and the instrumental colors should contain binaries, and so the effect will average to zero over many fields. While this may be true statistically, if the stars drawn from an observed field are few in number, the observed stellar locus may be distorted by small number statistics.

Another approach is to iteratively excise stellar colors that are significantly different from the standard color expectation. This should suppress locus shape distortions due to the occasional unresolved binary, but nevertheless the incidence of binary outliers is expected to be low. Smolčić et al. (2004) have shown the existence of an “echo” of the stellar locus, which they ascribed to unresolved binaries of similar luminosity but different effective temperatures. They assessed the number of objects in this “echo locus” as being fewer than 1/2000 as numerous as the objects that occupy the main stellar locus. The combined low incidence and known location of these outliers makes these binaries unproblematic.

#### 2.6. Variable Stars

Photometric variability is a source of systematic error for stellar locus color methods. If a star’s observed brightness varies in the time between observations in the various passbands under analysis, even if the underlying stellar color does not vary, the magnitude differences will introduce a shift in color-color space. Since the SDSS photometric data in different bands are obtained within a few minutes of each other, the SDSS-band standard stellar locus should have minimal contamination from this effect. Similarly, the 2MASS instrument obtained  $J$ ,  $H$ , and  $K$  photometry essentially simultaneously. Combining 2MASS and SDSS photometry, however, can fall prey to variability, since the observations were taken at different times. So establishing the joint optical/NIR standard stellar locus must attend to this issue.

Similarly, if the images under analysis are obtained at different times, variability on this timescale will distort the derived calibration color shifts. Sesar et al. (2007) explored the incidence of variables in the SDSS color-color diagram. They showed that there is a substantial variation in the fraction of objects that exhibit variability, across the color-color diagram. The blue tip of the stellar locus has two classes of variables: low redshift QSOs and RR Lyrae stars. These can be suppressed by selecting a judicious region in color-color space where the standard locus is matched to the instrumental color distribution, iteratively.

The multi-epoch analysis of SDSS photometry in Sesar et al. (2007) indicates that fewer than 5% of the objects in the main stellar locus exhibit variability with  $\Delta g > 0.05$  mag. A sigma-clipped iterative analysis of multi-epoch photometry should be able to produce a cleansed standard stellar locus.

#### 2.7. Galactic Dust

Galactic dust is another extrasolar source of stellar locus perturbations. The dust is shown by Marshall et al. (2006) and Jurić et al. (2008) to be confined to a sheet roughly 100 pc above and below the Galactic midplane. At SDSS depths, the vast majority of stars are therefore behind the dust.

To first approximation the extinction obeys the canonical  $R_V = 3.1$  reddening law and the degree of extinction  $A_V$  follows the maps of SFD. This induces a simple overall color-color vector shift—reddening—whose direction depends on  $R_V$  and whose magnitude depends on  $A_V$ . Ivezić et al. (2007) showed that the stellar locus position reflects these predictions in some regions of SDSS Stripe 82, but breaks down as Galactic latitude  $|b|$  decreases (§4.1).

The usual adoption of extinction coefficients from the SFD appendix assumes an underlying spectral energy distribution typical of an elliptical galaxy. This is not valid for Galactic stars (eg McCall 2004). To next approximation, a more correct treatment would provide extinction coefficients for each stellar spectral type. Errors of this form induce differential distortions of the stellar locus as a function of effective temperature.

Other deviations occur when the basic assumptions of extinction behavior break down. If the reddening law is not strictly  $R_V = 3.1$  (eg Larson & Whittet 2005), the stellar locus shifts in different directions. If some observed stars are in front of the dust and others behind, the stellar locus will show additional scatter, preferentially in the reddening directions. Because the stars are most often behind the dust, Galactic extinction is a major contributor to the observed stellar locus properties.

The SLR approach makes no specific assumption about any value of  $R_V$ . It corrects for Galactic extinction subject to the assumption that the observed stars all lie behind a *common* Galactic extinction layer. We suspect a fruitful approach might be to make an initial adjustment to the instrumental colors using SFD and  $R_V = 3.1$ , and then run SLR on the resulting catalog.

### 2.8. Summary

Taking all this information together, we have clear expectations for what constitutes the typical observed stellar locus, and what factors change its observed position or shape.

Stars with  $r - i > 0.7$  are mainly faint M dwarfs in the disk, with correspondingly high metallicity. Since these objects are only visible out to  $\sim 1$  kpc, only metallicity variations in this local region of the Galaxy could perturb the kink region of the observed locus.

The stars blue-ward of the kink, however, are a magnitude-dependent combination of halo stars and disk main sequence stars. The metallicity dependence of this region of the locus is small.

While the location of the bluest terminating edge of the stellar locus is an indicator of the age of the underlying population, it does not distort the basic shape of the locus line.

Galactic dust should be a prime source for locus shifts and possibly small distortions. At high Galactic latitudes the vast majority of SDSS stars reside behind the dust lanes of the Milky Way. At low Galactic latitudes, even distant stars come closer to the Galactic plane. We would therefore expect to eventually see a smearing of the stellar locus due to stars suffering different amounts of extinction along the line of sight.

Finally, atmospheric and instrumental effects will naturally perturb the stellar locus, and we model these in our mathematical formulation of Stellar Locus Regression (§3). Given what we have learned about the nature

of the observed stellar locus, our conception of SLR begins with a simple set of assumptions.

1. The standard stellar locus is representative of the typical stellar populations that we will observe in practice, and is sufficiently uniform so as to constitute a calibration standard. The standard locus stars:
  - (a) are disk dwarfs in the red and both disk and halo stars in the blue, thanks to the dramatic color-volume effects at SDSS depths, and
  - (b) lie at high enough Galactic latitude to put them behind the dust, but suffer low dust extinction.
2. Stars we observe in practice are always *behind* the Galactic dust sheet. This way, SLR directly outputs dereddened colors.
3. The Galactic dust extinction can obey *any* power law  $R_V$ .
4. The Galactic dust extinction is locally smooth.
5. Observations include the  $g$ -band, and are deep enough to observe at least a few of the faint M dwarfs that constitute the kink feature (limiting  $g \gtrsim 18$  mag, Ivezić et al. 2008).
6. The input images from which instrumental photometry is extracted are properly flat-fielded.

Many of these are testable in isolation (§4), but some possibly degenerate effects, such as simultaneously anomalous metallicities and extinction laws, may be difficult to disentangle. We deduce nonetheless that the combination of magnitude dynamic range selection effects and the relative insensitivity of the  $grizJHK$  stellar locus to stellar metallicity, age differences, and binary and variable contamination produces an observed stellar locus that is uniform enough to achieve calibration of colors using a standard stellar locus.

## 3. THE METHOD

The basis of Stellar Locus Regression is to transform instrumental stellar colors so that they align with a standard locus, on the SDSS photometric system. This requires typical data preprocessing and photometry that produces instrumental stellar colors from single-epoch, flat-fielded images. The only calibration images required for SLR are a single set of multiband observations of a high-density standard star field, from which instrumental color terms are measured. Periodic updates to the instrumental color terms will depend on the timescale over which these terms evolve. Mosaic imagers will benefit from chip-by-chip color terms. Then, with fixed color terms applied, SLR calibrations are performed on science frames by iteratively transforming the instrumental stellar colors to optimize a goodness-of-fit (GOF) statistic. The resulting best-fit parameters, including the instrumental color terms, define the color transformation that achieves the SLR calibration. Uncertainties in the calibration are estimated numerically. These calibration terms are then applied to all the cataloged photometry of

objects appearing in the same images. This way all objects in the field are calibrated using the same stars lying in that field, and no spatial nor temporal interpolation is required.

In this section we describe and motivate our calibration equations, discuss our chosen GOF and method of error estimation, and outline a practical algorithm that we have implemented for the real-time calibration of *griz* colors.

### 3.1. Color Transformations

A *color transformation* is the mathematical transformation of colors by translations, scalings, rotations and shears. Instrumental colors are represented with the vector<sup>7</sup>  $\mathbf{c}$ , and “true” colors, which we take to be on the SDSS photometric system, are represented with the vector  $\mathbf{c}_0$ . Instrumental colors relate to the true colors via the color transformation equation

$$\mathbf{c} = \boldsymbol{\kappa} + (\mathbf{1} + \mathbf{B})\mathbf{c}_0. \quad (1)$$

The color translation vector  $\boldsymbol{\kappa}$  accounts for first order atmospheric extinction, Galactic extinction, zeropoints, and any other additive effects, *known or unknown*. We discuss  $\boldsymbol{\kappa}$  in §3.2. The color term matrix  $\mathbf{B}$  is populated by zeros and constants, typically small, and corresponds to the instrumental color terms from conventional photometric calibrations. We discuss  $\mathbf{B}$  in §3.3. Appendix A shows in mathematical detail how Equation (1) relates to photometric calibration equations that astronomers typically adopt.

### 3.2. The Color Translation Vector

The color translation vector  $\boldsymbol{\kappa}$  accounts for differences of zeropoints  $a$ , atmospheric extinction  $E$ , and Galactic extinction  $A$ . The scalar elements of the translation vector are

$$\kappa_{nm} = a_n - a_m + E_n - E_m + A_n - A_m. \quad (2)$$

where  $n$  and  $m$  are elements of the filter set, for example  $n, m \in \{g, r, i, z\}$ , and  $n \neq m$ . See Appendix A for a derivation of this relation, starting from traditional photometric calibration equations.

In traditional photometric calibration, the terms on the right-hand side of Equation (2) are estimated independently. Atmospheric extinction is usually modeled using a Bouger extinction law,  $k_n X_n$ , where  $k_n$  is a filter-dependent constant and  $X_n$  is the airmass through which the  $R$ -band image was taken. The atmospheric extinction constants are extracted using intermittent standard star observations at a range of airmasses and interpolated in space and time to the science frames. This assumes that the linear airmass model reflects truth and is spatiotemporally invariant. Galactic extinction is normally estimated from SFD—a procedure that assumes a single  $R_V = 3.1$  dust reddening law (cf. Schlegel et al. 1998). Finally, zeropoints are estimated using the same standard star frames used to measure the atmospheric terms. The zeropoints standardize the photometry, and account for differences in instrumental throughput between facilities and any other unmodeled additive effects.

<sup>7</sup> Our convention is to assign vectors boldface, lowercase letters, and matrices boldface, capital letters. The *elements* of vectors, matrices, and tensors, like all scalars, are not boldface.

Zeropoints are then interpolated in space and time to the science frames in “photometric conditions,” which again assumes spatiotemporal invariance.

SLR is fundamentally different and is not subject to these assumptions. SLR fits for each element of the vector  $\boldsymbol{\kappa}$  directly, and therefore calibrates the entire right-hand side of Equation (2) in one step. The atmospheric and dust extinctions and the zeropoints are not estimated independently. This is made possible by the universality of colors of abundant MS stars (§2). Because of this unique ability of SLR, *it does not matter what mathematical form the extinction and zeropoint terms take in reality, as long as they are additive, because all additive systematic effects are accounted for together by  $\boldsymbol{\kappa}$  during SLR*. For example, the Bouger atmospheric extinction law is likely incorrect in the  $z$ -band, where water absorption is saturated and the additive airmass dependence probably better follows an  $X_z^{1/2}$  airmass power law (cf. Stubbs et al. 2007). Further, as we have mentioned it is probable that not all Galactic dust columns obey the canonical  $R_V = 3.1$  extinction law. SLR is immune to additive mis-modeling of the atmosphere, Galactic dust, overall instrument sensitivity differences, aperture corrections, and so on.

Figure 1 demonstrates the effect of leaving the color translation vector free during Stellar Locus Regression. The top panels show how the known, standard locus compares to an instrumental stellar locus. In the middle panel, we perform SLR, letting  $\boldsymbol{\kappa}$  be free and fixing the color term matrix  $\mathbf{B}$  to zero. Residual systematics are clearly evident, in the form of deviations that appear to increase with color. This is expected because we are comparing standard SDSS data to data taken with a different instrument than SDSS. We remedy this by measuring color terms for the instrument once using a standard stellar field observation, and then fixing these nonzero color terms while performing SLR. Color term issues are described in the following section.

### 3.3. The Color Term Matrix

The entries of the color term matrix  $\mathbf{B}$  are zeroes or constants. For example, for the SDSS colors we use in §4.2-4.4,  $\mathbf{c} = (g - r, r - i, i - z)$ , we adopt the color term matrix

$$\mathbf{B} = \begin{pmatrix} b_g & -b_r & 0 \\ 0 & b_r & -b_i \\ 0 & 0 & b_i - b_z \end{pmatrix}. \quad (3)$$

This has a direct correspondence with traditional photometric color term formulations, as shown in Appendix A.

Color terms, and the color term matrix, account for broad, differential instrument sensitivity differences that arise when data are acquired with different telescopes, CCDs, or filters than those used to generate the standard catalog. For example, we see a clear systematic error between IMACS and SDSS in Figure 1 that varies monotonically with color. By estimating color terms with an observation of a standard star field and applying the color term matrix transformation during our SLR, we significantly improve the fit.

We have also estimated color terms directly with SLR by letting the color terms be free in addition to  $\boldsymbol{\kappa}$  during the fit. This results in a divergent regression when using

our weighted color residual GOF (§3.6). The reason is that the global minimum of this GOF occurs when all instrumental data points collapse to a single point, which is allowed by divergent shears and rescalings from  $\mathbf{B}$ , and divergent, compensatory color translations that put the singular instrumental data somewhere on the standard locus line. The best-fit color terms are extremely large, violating our assumption of smallness. We have experimented with other GOFs with varying success, but none yields color terms with accuracy that rivals that of the traditional procedure.

This is the only step in our real-time color calibration procedure (§3.8) that requires standard star observations. If instrumental color terms are stable over, say, month- and year-long timescales, then color terms need only be estimated as infrequently. Without the requirement of multiple standard field exposures per night, the observer maximizes the total exposure time on science fields.

### 3.4. Color-Airmass and Higher Order Corrections

Color-airmass terms take the same essential form as instrumental color terms. Appendix A gives an explicit example of this. Correspondingly, color-airmass terms can be estimated with the same color term procedure described in §3.3 and §3.8. We have not yet implemented this as we assume these corrections to be small; this is an obvious future addition to our SLR formulation. In principle, corrections proportional to higher order powers of the color, airmass, and even the Galactic dust column can also be measured, but these will require larger, dedicated programs in order to minimize error. As shown in §4.2-4.4, we achieve 1–2% level self-consistency with respect to zeropoints, airmass, and Galactic dust, without making these corrections.

We now show how, using the same formalism and the same standard locus of §2.1, SLR can be made to output individual calibrations for each filter, producing calibrated photometry instead of colors.

### 3.5. Photometric Calibration with SLR Using 2MASS

If the stellar locus is extended into other passbands that are already photometrically calibrated, then the instrumental photometry can be directly calibrated using only the SLR methodology. 2MASS is an obvious choice for an external catalog, as it is full-sky and freely available and the standard locus (§2.1) bridges *JHK* with *ugriz*.

The procedure requires the additional prior step of cross-correlating instrumental stellar catalogs against 2MASS’s calibrated data. This is easily done using the Gator web interface<sup>8</sup>.

For illustration, say we have obtained the *J*-band photometry of our instrumental *griz* stars. We construct a color that is a hybrid of instrumental optical magnitudes and calibrated 2MASS magnitudes,  $z - J$ , which extends the instrumental stellar locus to  $\mathbf{c} = (g - r, r - i, i - z, z - J)$ . SLR is executed in precisely the same way as for the optical data alone, using the standard optical-infrared hybrid locus line. The result is still  $\kappa$ , but the last entry is  $\kappa_{zJ} = a_z + E_z + A_z$  because the 2MASS data are

already calibrated:  $\kappa_{zJ}$  is the *z*-band photometric calibration. This can be done for any combination of instrumental calibrated 2MASS data and instrumental optical or infrared data from a different passband. Appendix A makes the mathematics of SLR photometric calibration explicit for this particular example.

SLR photometric calibration is subject to the errors of 2MASS, and is more precise when more stars are used in the fit. Given typical 2MASS errors of 5%, SLR-calibrated photometric zeropoints should typically be accurate to 5% or better. By the nature of SLR, the Galactic dust correction is inextricable from the photometric calibration when the instrumental stars are all behind the dust, so uncertainty from the dust must be added in quadrature. Finally, color terms carry with them additional uncertainty from the color term estimate and the colors that they multiply. If color terms are used, then the colors must be estimated independently from the the non-2MASS data, either simultaneously during the 2MASS fit or prior to it.

2MASS matches will probably only occur for a *subset* of one’s instrumental data. The reduced number of stars will generically degrade the Stellar Locus Regression errors. Our optimized procedure is to first perform an instrumental-only SLR to estimate the colors using a maximal number of stars, and, if the photometry is needed at all, to perform a 2MASS SLR on the subset of matches to calibrate the photometry separately. This ensures that the color errors are minimal and not subject to the errors from 2MASS and from the reduced statistics. SLR never requires the subtraction of calibrated photometry to arrive at colors.

### 3.6. Goodness of Fit

During Stellar Locus Regression we optimize goodness-of-fit (GOF) statistics and estimate errors numerically. The GOF statistic we have adopted is the weighted, perpendicular color-distance residual.

The perpendicular color-distance is a hyper-dimensional distance in color space between an instrumental data point and the nearest point on the standard locus line. Our standard locus line is a collection of closely-spaced data points, so we make numerical approximations to calculate the distance. As we make explicit below, we first compute all possible distances between the instrumental colors and the points on the standard locus line, then we find the minimum distance for each instrumental data point. Finally we sum the result.

Consider instrumental color data points  $\mathbf{c}_\alpha$ , where  $\alpha$  indexes the instrumental color data vector of each star. We compute the vector distances between every  $\mathbf{c}_\alpha$  and every data point on our standard locus line,  $\mathbf{c}_{0\beta}$ , where  $\mathbf{c}_{0\beta}$  is also an array of vectors and  $\beta$  varies along the standard locus line. These distances are  $\mathbf{d}_{\alpha\beta} \equiv \mathbf{c}_\alpha - \mathbf{c}_{0\beta}$ , where  $\mathbf{d}_{\alpha\beta}$  is a tensor of all possible distances between the instrumental colors and the points on the standard locus line.

We weight the distances either by the number 1 or by the color measurement uncertainty in the direction of the line connecting each pair of points  $\alpha$ - $\beta$ . Whether to weight by unity or by color uncertainties is at the discretion of the user. We take the norms of each weighted

<sup>8</sup> <http://irsa.ipac.caltech.edu/cgi-bin/Gator/nph-dd?catalog=frustrated>



distance vector, so our weighted distance measure is

$$|\mathbf{d}_{\alpha\beta}^w| = \frac{|\mathbf{d}_{\alpha\beta}|}{|\boldsymbol{\sigma}_\alpha \cdot \hat{\mathbf{d}}_{\alpha\beta}|}. \quad (4)$$

Here the dot product  $\cdot$  is taken between the vector of data uncertainties  $\boldsymbol{\sigma}_\alpha$  and the unit vector that lies along the pairs of points  $\hat{\mathbf{d}}_{\alpha\beta}$ . The quantity  $\boldsymbol{\sigma}_\alpha \cdot \hat{\mathbf{d}}_{\alpha\beta}$  is the uncertainty projected along the line that connects each pair of points.

Then, for each  $\alpha$ , we select the one  $\beta = \beta^*$  such that  $|\mathbf{d}_{\alpha\beta^*}^w| = \min(|\mathbf{d}_{\alpha\beta}^w|)$ . This is the closest distance to the standard locus line for the instrumental data point  $\alpha$ . We do this for all data points  $\alpha$ , and sum the results as

$$T = \sum_{\alpha} |\mathbf{d}_{\alpha\beta^*}^w|, \quad (5)$$

noting that there is one  $\beta^*$  for each  $\alpha$ . This is an estimate of the weighted distance residual between all instrumental data points and the standard locus line—a scalar.

Our SLR implementation produces best-fit calibration parameters by varying  $\boldsymbol{\kappa}$  and adding it to the instrumental colors, then recomputing  $T$ , and repeating this process until  $T$  is minimized. We use the amoeba downhill simplex method (Nelder & Mead 1965).

Our statistic was chosen for robustness.  $T$  would be equivalent to the  $\chi^2$  statistic if the distances were squared and weighted by the inverse variance<sup>9</sup>, but the square puts undue weight on statistical outliers. Likewise, using uniform weights of unity, the residual of square perpendicular distances becomes equivalent to the so-called “total least-squares” statistic. This similarly gives undue weight to *non*-statistical outliers. We wish to apply SLR to any data at the telescope, on the fly, so robustness to outliers is critical.

To insure doubly against outliers, we perform SLR twice. The first iteration gives rough estimates of best-fit calibration parameters, allowing us to excise stars we deem to lie too far away from standard locus line. We typically cut stars with color distance  $|\mathbf{d}_{\alpha\beta^*}| > 6|\boldsymbol{\sigma}_\alpha \cdot \hat{\mathbf{d}}_{\alpha\beta^*}|$  away from our standard locus line (a figure informed by Covey et al. 2007), and as well as those with  $|\mathbf{d}_{\alpha\beta^*}| > 1$  mag. We then perform SLR once more on the cleaned data.

### 3.7. Uncertainty Estimation

We estimate all uncertainties on best-fit parameters with the bootstrap method (Efron 1979). At each bootstrap iteration  $i$  we resample  $N_{\text{stars}}$  data points  $N_{\text{stars}}$  times with replacement to obtain a bootstrap sample, and perform the GOF optimization described above on the new sample. This gives best fit parameters  $\boldsymbol{\kappa}_i$ , which we record. We repeat this  $N_{\text{boot}} \sim 100$  to 1000 times, obtaining  $N_{\text{boot}}$ -size arrays of each vector  $\boldsymbol{\kappa}_i$ . The mean of each bootstrap distribution is an estimate of the sample mean of each parameter. The standard deviation of the bootstrap distribution is an estimate of the standard error on the mean.

<sup>9</sup> In this case our GOF is closely related to the 7-dimensional color distance of Covey et al. (2007). The difference is that we weight by the errors in the direction of the line connecting the data and the nearest point on the standard locus line.

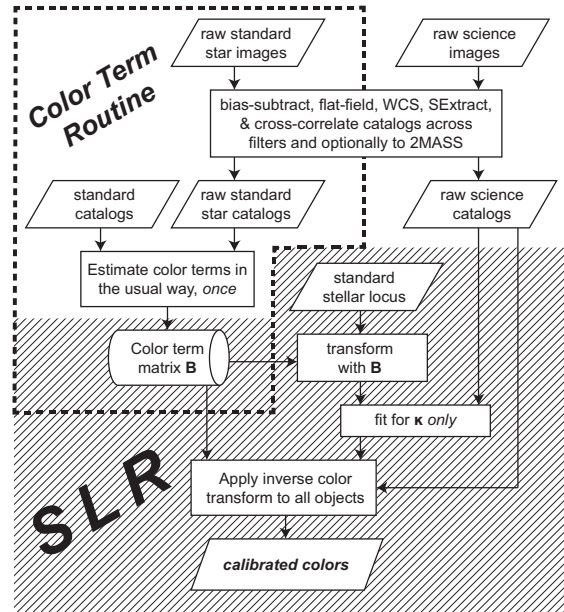


FIG. 3.— SLR flow chart for calibrating colors. The hashed region denotes parts of the algorithm that are unique to SLR, while the non-shaded region shows steps that are more traditional. The dotted region denotes the color term estimation routine, which need only be performed once per detector.

This approach means that to estimate uncertainties we repeat the entire stellar locus regression  $N_{\text{boot}}$  times. This can be time-prohibitive for large samples, but we argue it is not always necessary to repeat the error estimation after it has been performed once. If different stellar images are taken from the same instrument under similar circumstances, and if the bootstrap distributions are roughly normal, then errors for different size data sets can be estimated with rescaling by  $\sqrt{N_{\text{stars}}}$ . This estimate may break down if those assumptions do not apply, but we argue  $\sqrt{N_{\text{stars}}}$  rescaling can give errors to a factor of a few for  $N_{\text{stars}}$  that are not wildly different. We now describe the full algorithm we have implemented to produce calibrated colors from flatfielded images.

### 3.8. An Algorithm

We have developed an optimized algorithm that produces SLR-calibrated colors from flatfielded images, essentially in real time. It is schematically outlined in Figure 3. The data undergo standard preprocessing, color terms are determined in the normal way from standard star frames *once*, and SLR fitting is done subsequently on all science frames.

SLR requires single-epoch multiband observations of any number of science fields and one standard star field. All images are bias-subtracted, flat-fielded, WCS-registered, and Source Extracted. The resulting instrumental catalogs from each passband are cross-correlated with one another to find the unique objects, and point-sources are identified, for example, using Source Extractor’s CLASS\_STAR parameter. All stars are required to be unambiguously identifiable in all bands, and at all stages we only consider those with signal-to-noise  $> 10$ .

Instrumental color terms are then determined once only from the standard star field, in the traditional way. For example, following the equations of Appendix A we estimate the  $g$ -band color term  $b_g$  as the slope of the

best-fit line to  $g - g_0$  vs.  $g_0 - r_0$ , and so forth for the rest of the passbands. The color terms are stored as the color term matrix  $\mathbf{B}$ .

With color terms in hand, real-time SLR calibration of any number of science fields can be undertaken. The color terms are first applied to the standard stellar locus with the transform  $(\mathbf{1} + \mathbf{B})$ , bringing the standard locus into *standardized instrumental color space*. In this space, the instrumental stellar colors from the flat-fielded science images are regressed to the standard locus, leaving only the color translation vector  $\boldsymbol{\kappa}$  free. This stage can be executed as soon as flat-fielded multiband images are in hand. Flat-fielding and object cataloging can be performed at the telescope during observation, so Stellar Locus Regression is viable as a real-time calibration technique.

The instrumental science catalog of both point-like and extended sources is calibrated by applying the inverse color transformation,

$$\mathbf{c}_0 = (\mathbf{1} + \mathbf{B})^{-1} (\mathbf{c} - \boldsymbol{\kappa}). \quad (6)$$

$\mathbf{B}$  was determined from the standard star observations, and  $\boldsymbol{\kappa}$  was obtained from the SLR. The transform  $(\mathbf{1} + \mathbf{B})$  is invertible under normal circumstances of small color terms (see Appendix A).

As outlined in §3.5, SLR generates calibrated magnitudes using 2MASS entries using exactly the color calibration process described above, with judicious choices of color vector entries. The additional step of matching one’s instrumental objects to 2MASS lasts seconds to minutes for typical catalogs containing of order tens to hundreds of stars.

We apply this algorithm to real data in a series of test, presented in the following section.

#### 4. FIRST TESTS

We employed the algorithm of §3.8 on existing, calibrated SDSS data and on new *griz* data we have acquired on the 6.5 m Magellan telescopes using the IMACS (Dressler et al. 2003; Osip et al. 2008) and LDSS3 (see Osip et al. 2008) instruments in imaging mode. We designed a series of tests to isolate the effect of Galactic extinction and airmass and to generally assess the reproducibility of colors using SLR. Finally, we used SLR in a measurement of redshifts of 11 galaxy clusters using colors alone.

##### 4.1. Galactic Extinction

The majority of SDSS stars at high Galactic latitude are expected to be behind the dust (§2), so we designed a simple test of SLR to measure the extinction directly. We applied SLR to ubercalibrated (Padmanabhan et al. 2008) SDSS stars subject to varying degrees of predicted reddening, and compared the results to SFD expectation. Ubercal SDSS data are calibrated to the top of the atmosphere, in front of the Galactic dust. We therefore expect the best-fit color vector  $\boldsymbol{\kappa}$  to be equal to the reddening vector, especially at high Galactic latitudes, and we expect the canonical  $R_V = 3.1$  extinction law to hold.

We began by querying photometric quality ubercalibrated SDSS point sources from the CasJobs web server<sup>10</sup>. Photometric quality ubercalibrated colors are

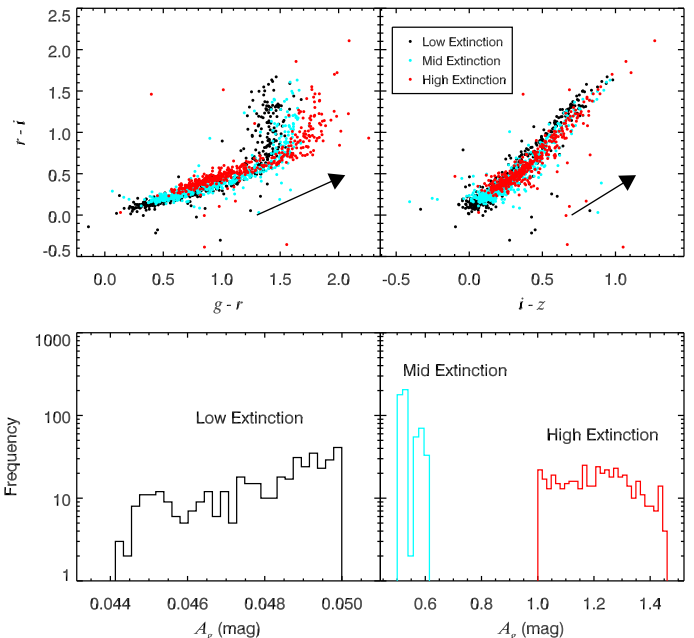


FIG. 4.— Three samples of SDSS stars with different ranges of predicted Galactic extinction (low:  $A_g \sim 0.05$  mag, intermediate:  $A_g \sim 0.5$  mag, and high:  $A_g \sim 1.2$  mag). *Top panels*: color-color stellar loci, shown with the canonical reddening unit vector in three-dimensional color space. *Bottom panels*: histograms for predicted  $g$ -band Galactic extinction.

accurate over a wide area of the sky, with 1.5% estimated uncertainty, so this is the ideal SDSS data set to perform our test on, in terms of size and quality. We queried stars in small ranges of SFD-predicted extinction and performed multiple such queries over a wide range of mean extinctions. The results were samples of hundreds of stars each in finite Galactic extinction bins over a wide range of SFD dust columns. We selected stars with signal-to-noise ratio  $> 10$  in all bands to minimize uncertainty from poor color measurement.

Figure 4 displays three of these data sets. Low ( $A_g \sim 0.05$  mag), intermediate ( $A_g \sim 0.5$  mag), and high ( $A_g \sim 1.2$  mag) Galactic extinction ranges were queried, as shown in the figure. Histograms of the SFD-predicted extinction in the  $g$ -band for each star show that these extinction distributions are localized and well separated. The gross effect of Galactic reddening is readily apparent in color-color diagrams (top panels).

In total we acquired 7 such data sets, sampled from the northern and southern Galactic hemispheres, probing mean  $A_g$  between 0.05 and 1.2 mag. By nature of the SDSS database organization and the available data itself, the data sets happen to come from fields that are localized to  $\sim 1$  deg<sup>2</sup>, except for one. The Galactic coordinates are given in Table 3. The last field in Table 3 shows a wide range of stellar coordinates because the CasJobs query, by chance, returned stars spread over a few disjointed regions of the sky.

We performed Stellar Locus Regressions on each data set. We fixed the color term matrix  $\mathbf{B}$  to zero because this test involved comparing a standard stellar locus standardized to the SDSS photometric system, to col-

<sup>10</sup> <http://casjobs.sdss.org/CasJobs/>

TABLE 3  
GALACTIC EXTINCTION FIELDS.

Mean $A_g$ (mag)	$\ell$ (deg) <sup>a</sup>	$b$ (deg) <sup>b</sup>
0.048	$57.9 \pm 1.0$	$37.9 \pm 0.5$
0.538	$15.8 \pm 0.2$	$29.0 \pm 0.2$
1.210	$11.4 \pm 0.1$	$36.2 \pm 0.1$
0.090	$130.6 \pm 0.9$	$-49.0 \pm 0.2$
0.268	$115.2 \pm 0.4$	$-48.7 \pm 0.1$
0.727	$149.8 \pm 0.4$	$-46.6 \pm 0.1$
1.068	$56.6 \pm 33.9$	$-37.5 \pm 3.1$

<sup>a</sup> Mean and standard deviation of Galactic longitudes for stars in the sample.

<sup>b</sup> Mean and standard deviation of Galactic latitudes for stars in sample.

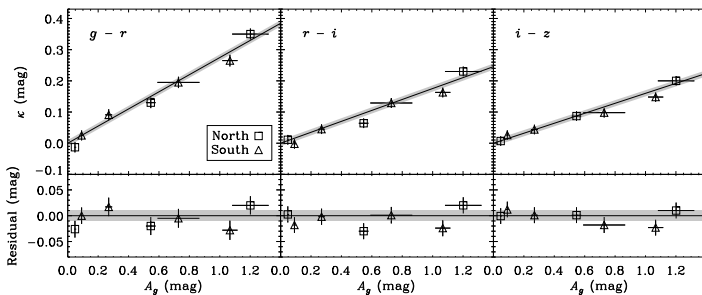


FIG. 5.— Best-fit color shifts  $\kappa$  vs. predicted Galactic extinction in the  $g$ -band, and residuals. The solid lines are the SFD-predicted reddening corresponding to the  $g$ -band extinction given on the abscissa. Northern and southern Galactic hemisphere fields are indicated, and the  $\pm 10$  mmag region is shaded.

ors generated by the SDSS instrument itself. After our restrictions on the data were enforced (see §3.6), between 380 to 490 stars from each data set were ultimately used in the fits. The best-fit color shifts  $\kappa$  that resulted are directly compared to the SFD-predicted reddening in Figure 5. The expectation, if our hypotheses hold, is that  $\kappa$  will be equal to the reddening vector.

The solid lines in Figure 5 show the *predicted* color-reddening values  $A_n - A_m$ ,  $n, m \in \{g, r, i, z\}$  corresponding to the predicted  $g$ -band extinction given on the abscissa, assuming the canonical  $R_V = 3.1$  reddening law. The error bars for the abscissa are the standard deviation of predicted extinction values for the corresponding data set. Error bars for the ordinate are the standard error on the mean predicted reddening added in quadrature to the bootstrap errors of SLR and the 1.5% color uncertainty limit to which overcalibrated colors are subject.

The best-fit color shifts from SLR are consistent with Galactic reddening within the errors for these data, with residual RMS of 19 mmag in the color  $g - r$ , 18 mmag in  $r - i$ , and 13 mmag in  $i - z$ . The maximum residual disagreement is 30 mmag in  $g - r$  and  $r - i$ , and 19 mmag in  $i - z$ .

Ivezić et al. (2007) performed a similar analysis in SDSS Stripe 82 with their “stellar locus method,” showing maximum sensitivity to the magnitude of SFD extinction at roughly the 20 mmag level at high Galactic latitudes. Their measurements showed disagreement with SFD prediction at Galactic latitudes  $|b| \sim 40$ –50 deg and below (their §2.7.1). Our results probed latitudes in this range and lower, but in fields from different Stripes, so

our results are not inconsistent with theirs. In other tests (§4.2), we observed Stripe 82 fields where their stellar locus method failed, and we reproduced their results. Taking this information together, we conclude that stellar locus methods *can* reproduce the  $R_V = 3.1$  reddening law in both magnitude and direction, even through significant dust columns, so dust thickness alone is not a good indicator of SLR reliability.

#### 4.2. Color and Magnitude Reproducibility

We tested the ability of SLR to reproduce colors and magnitudes using data acquired at different telescopes. We chose Stripe 82 fields because of the high quality, 1% photometry available from Ivezić et al. (2007). We probed fields that contained among the highest densities of stars in the entire Stripe 82 in order to minimize statistical uncertainty. The stars in these regions, however, are known not to reproduce the SFD extinction prediction with stellar locus methods (§2.7.1 of Ivezić et al. 2007). The possible reasons cited were an invalid extinction law  $R_V$ , a drift in mean metallicities, or dust that was both in front of and behind the stars. Nonetheless, we designed our experiment to control for the anomalous dust, as described below, so that we could study in isolation SLR’s fundamental ability to reproduce colors and magnitudes when applied to data from different instruments.

In 2008 we undertook observing programs at the 6.5 m Magellan telescopes using the IMACS instrument in imaging mode. We observed three, high stellar density Stripe 82 fields, which we label S1, S2, and S3. Our field S1 is centered at  $(\ell, b) = (48.65151, -26.04729)$  deg, S2 at  $(\ell, b) = (51.86849, -33.74441)$  deg, and S3 at  $(\ell, b) = (50.43107, -30.24483)$  deg. These fields are all at lower Galactic latitude  $|b|$  than those of §4.1, except for the second field shown in Table 3. Each IMACS CCD is  $4' \times 8'$ , arranged in two rows of four. Just as we have described in §3.8, we flat-fielded the data and produced instrumental, multiband catalogs. We associated stars between passbands by requiring their positions to agree to better than  $1''$  in radius. We then found the corresponding photometry in the catalog of Ivezić et al. (2007) in the same way, selecting only those stars with more than 4 SDSS observations per passband and with signal-to-noise  $> 10$ .

In order to compare the colors of stars directly, we treated the SDSS catalog data as pseudo-IMACS observations: we extracted only the stars that also appeared in the 8 IMACS CCDs, in all  $griz$  bands. This was repeated for the three fields. Because we wished to compare SLR magnitudes in addition to colors, we also found the 2MASS  $J$ -band photometry for the stars. Of order 10–100 stars per CCD per field were matched across the IMACS, SDSS, and 2MASS data sets.

Following the procedure outlined in §3.3 and §3.8, we measured the IMACS color terms from the SDSS standard stars. We exploited the fact that we observed 3 standard fields, and measured color terms independently in all of them, one CCD at a time, taking the average of the result. We applied the same mean color term correction to all CCDs. This color term procedure gave smaller color and magnitude residuals than (1) using different mean color terms for each CCD and (2) using separate color terms for each field *and* CCD.

First, we ran SLR to calibrate only the colors. We controlled for the anomalous stellar locus shifts by regressing

both the calibrated SDSS data and our instrumental colors to the standard locus line. The best-fit  $\kappa$  for the SDSS data showed color translations that disagreed with SFD prediction by  $\sim 50$ – $100\%$ , consistent with the findings of Ivezić et al. (2007). By applying SLR to both the instrumental and SDSS data sets, we effectively canceled the anomaly by subtraction.

In a separate, subsequent step we calibrated the photometry using SLR, fixing the optical-only color shifts to those measured in the first step, as described in §3.5 and §3.8. We solved for the SLR-standardized photometry as

$$g_0 = g - \kappa_{gJ} - b_g(g_0 - r_0) \quad (7a)$$

$$r_0 = r - \kappa_{rJ} - b_r(r_0 - i_0) \quad (7b)$$

$$i_0 = i - \kappa_{iJ} - b_i(i_0 - z_0) \quad (7c)$$

$$z_0 = z - \kappa_{zJ} - b_z(i_0 - z_0) \quad (7d)$$

where the color terms  $b_n$  were the measured values for the IMACS catalogs, and zero for the SDSS catalogs. For the colors on the right-hand side, we used the SLR calibrations from the first, optical-only color iteration. The  $\kappa_{gJ}$ ,  $\kappa_{rJ}$ , etc, were those obtained from the second, optical-infrared magnitude iteration of SLR.

Figures 6 and 7 show the resulting color and magnitude residuals. The figures show a lack of pronounced systematic error in SLR colors as a function of effective temperature,  $g - i$ . We assess that colors calibrated purely with SLR are reproducible between the SDSS and the IMACS instruments to (18, 6, 5) mmag in the colors ( $g - r$ ,  $r - i$ ,  $i - z$ ). Magnitudes obtained only with SLR, using 2MASS, are reproducible between IMACS and SDSS to (44, 25, 19, 9) mmag in the ( $g$ ,  $r$ ,  $i$ ,  $z$ ) passbands. These numbers do not include the Galactic dust uncertainty because we applied SLR to both data sets, but they do necessarily include the intrinsic airmass correction that SLR makes. Our following test isolated completely the effect of the atmosphere using IMACS data alone.

### 4.3. The Atmosphere

We again tested the reproducibility of SLR-calibrated colors, this time isolating and varying the effect of atmospheric extinction. An advantage to the SLR approach is that it does not assume any particular functional dependence of color variation with airmass (§3.2). We therefore expect precise airmass corrections from SLR.

We isolated the effect of the atmosphere by performing SLR on the *same sets of stars* observed through 2 different airmasses using the same instrument, and compared directly the SLR-calibrated colors of the matched stars. We observed the IMACS fields described in §4.2 through multiple airmasses with the *griz* passbands. We included two additional fields, S5 at  $(\ell, b) = (122.46159, -63.21097)$  deg and CL1 at  $(\ell, b) = (96.07818, -61.31761)$  deg—the latter of which we observed at three different airmasses. The field S5 is in Stripe 82, but did not contain enough matches between IMACS, SDSS, and 2MASS to include in the analysis of §4.2. The field CL1 is not in the SDSS footprint.

The data preprocessing was identical to that of §4.2, except here we applied the nonzero color term corrections to all IMACS data, and we did not cross-correlate with 2MASS as we only wish to examine colors.

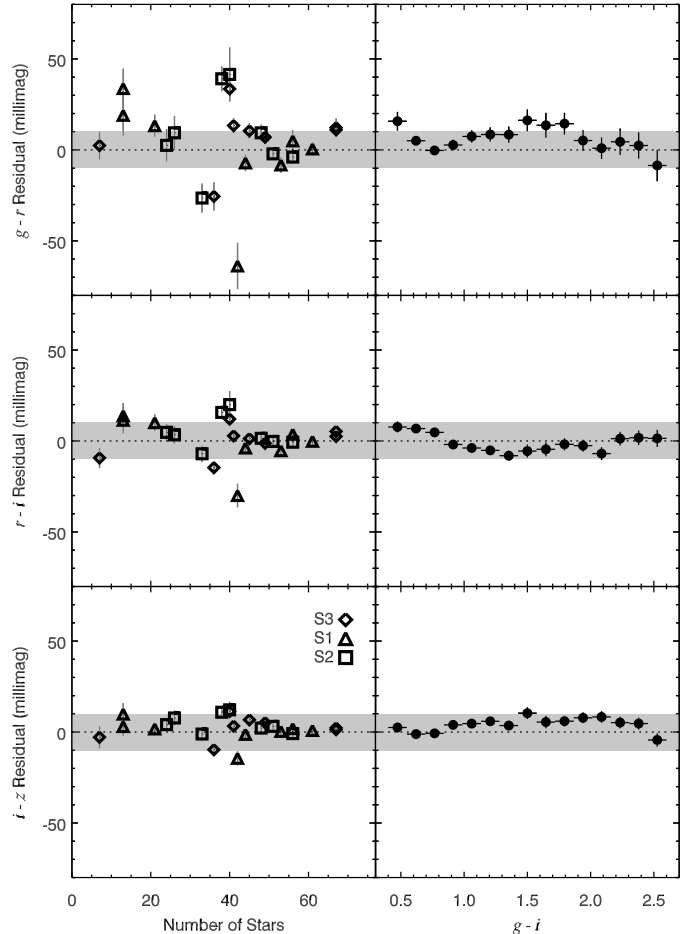


FIG. 6.— SLR color reproducibility, where SLR was applied both to SDSS and new IMACS observations. Color residuals are plotted vs. number of stars used per SLR (*left panels*) and vs. true  $g - i$  color (*right panels*). Each data point on the left represents an SLR calibration done on one CCD, and residuals vs.  $g - i$  are averaged over the union of all stellar residuals across all fields and CCDs. The  $\pm 10$  mmag region is shaded.

Figure 8 shows the results. The left panel shows the weighted mean residuals of stellar colors per CCD per field, with bootstrap errors, plotted against the number of useful stars extracted from each CCD. The right hand panel shows the mean of each set of 8 data points per field, with error bars reflecting the RMS scatter, plotted vs. the airmass ratio of the two observations. CL1 was observed at three airmasses, and the highest two airmasses are each paired with the lowest airmass in this figure.

This shows that SLR colors are reproducible over a wide range of airmasses, with residual RMS scatter in ( $g - r$ ,  $r - i$ ,  $i - z$ ) of (14, 8, 5) mmag when the number of stars used is  $> 30$ , and (20, 10, 8) mmag overall. Color errors do not correlate well with increased airmass. As is expected, there is a dependence of the color errors on the number of stars used per regression. The reduced  $\chi^2$  of the fits are roughly in the range [1, 3], with larger values for bluer bands. The larger  $N_{\text{stars}}$  data exhibit slightly larger  $\chi^2$ , and smaller  $N_{\text{stars}}$  data exhibit slightly smaller  $\chi^2$ . This suggests that the bootstrap slightly overestimates errors at small  $N_{\text{stars}}$ , and slightly under-

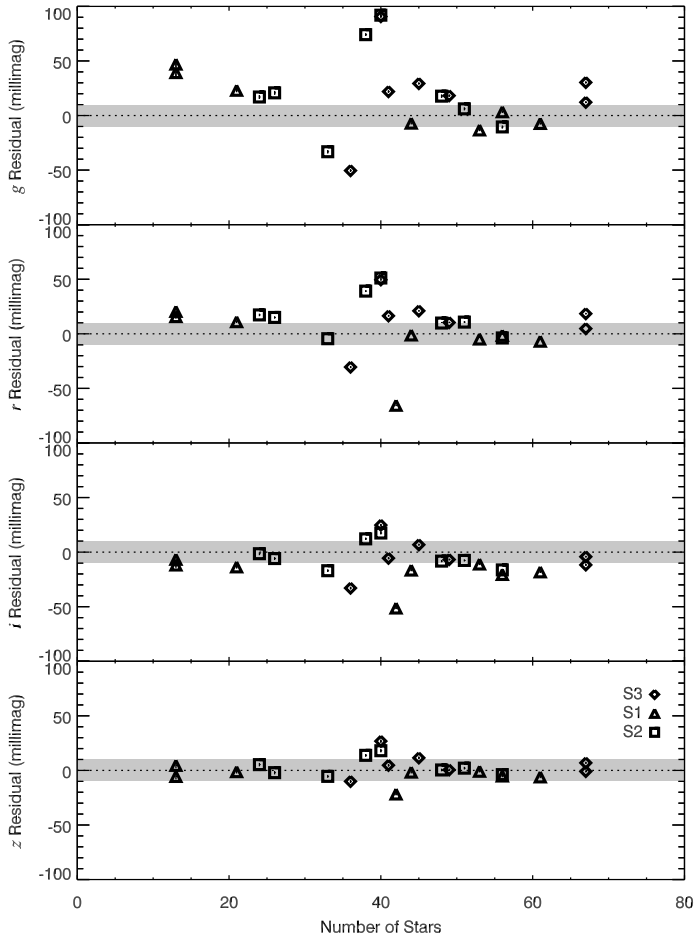


FIG. 7.— SLR magnitude reproducibility, where SLR was applied both to SDSS and new IMACS observations. A 2MASS SLR magnitude calibration was performed, again on both data sets as in Figure 6, with one data point per CCD. The  $\pm 10$  mmag region is shaded.

estimates errors at larger  $N_{\text{stars}}$ . This may be due to mildly non-Gaussian distributions. Overall, these results suggest that SLR systematic errors are not dominated by airmass issues for the fields we tested, but instead are dominated by the statistical noise inherent to the method as applied to the particular data we have used it on here.

As our final test, we deployed SLR colors in a photometric redshift measurement, as distance estimation is one of the prime uses of accurately calibrated colors.

#### 4.4. Galaxy Cluster Redshifts

We used SLR-calibrated colors to recover the redshifts of galaxy clusters. As part of the 2008 observing program we mentioned in §4.2 and §4.3, we observed known galaxy clusters from the REFLEX catalog (Böhringer et al. 2004), primarily a subset that are also Abell clusters (Abell et al. 1989). These observations were acquired with the LDSS3 camera at the Magellan 6.5 m telescopes (see Osip et al. 2008) in imaging mode. Because the redshift of the clusters are known, this serves as a test of our color calibrations within the context of a full scientific analysis.

We estimated LDSS3 color terms using standard star fields. Individual SLR calibrations were then obtained

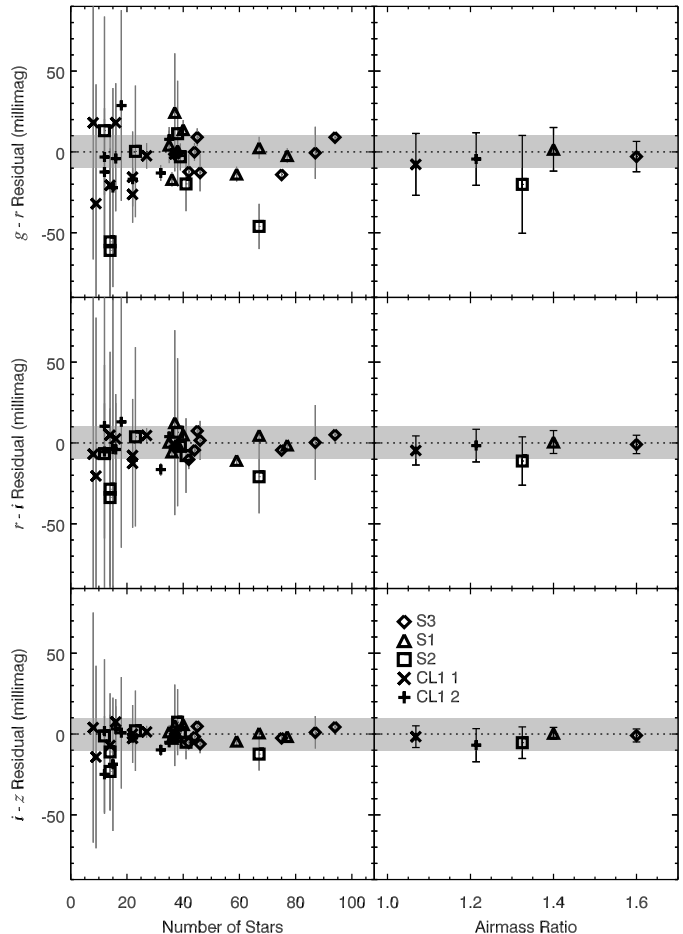


FIG. 8.— Color residuals between SLR calibrations of fields imaged with IMACS at different airmasses. The  $\pm 10$  mmag region is shaded. *Left hand plots:* Residuals vs. number of stars used to perform each SLR. *Right hand plots:* Mean of residuals over the 8 IMACS CCDs vs. airmass ratio between the two observations, and error bars are the RMS of residuals per field.

directly from each of the single-epoch *griz* cluster fields, and the  $\mathbf{B}$  and best-fit  $\kappa$  applied to the galaxy colors without applying any further corrections for airmass or Galactic extinction. We then selected the brightest red-sequence cluster galaxies from color-magnitude diagrams, spanning  $\sim 1$ – $2$  mag fainter than the brightest cluster galaxy (BCG) magnitude. This typically included of order 10 galaxies. We calculated the weighted mean of their  $g-i = (g-r) + (r-i)$  colors and estimated the cluster redshift with the empirical color-to-redshift tables of Lopes (2007). For the low redshift range we probed, the  $g-i$  color of red cluster galaxies varies rapidly and monotonically with redshift and is an ideal redshift estimator.

Table 4 summarizes the galaxy clusters we targeted, along with their Galactic coordinates and our results. The Abell systems 3693 and 3738 have been identified by previous authors as multi-redshifts systems. We were able to isolate the sub-systems using color-magnitude diagrams and image inspection, and we estimated their redshifts independently.

The results for the 11 clusters are plotted in Figure 9. The  $g-i$  cluster color errors  $SE_{gi}$  were estimated

TABLE 4  
SUMMARY OF THE CLUSTER DATA AND RESULTS.

Name	References <sup>a</sup>	Redshift Spec <sup>b</sup>	Redshift SLR <sup>c</sup>	Airmass <sup>d</sup>	Seeing <sup>e</sup> (arcsec)	$E_{g-i}$ <sup>f</sup> (mag)	$N$ stars <sup>g</sup>	$b^h$ (deg)
ABELL 3668	1, 2	0.1496	$0.156 \pm 0.011$	1.9	2.0–3.0	0.083	58	–32
ABELL 3675	1, 2	0.1383	$0.150 \pm 0.012$	1.9	1.8–1.9	0.079	67	–35
RXC J2023.4–5535	2	0.232	$0.238 \pm 0.012$	1.7	1.7–2.3	0.102	70	–35
ABELL 3693	1, 3, 4	0.091	$0.093 \pm 0.016$	1.5	1.8–3.0	0.060	62	–35
ABELL 3693	1, 4, 5	0.123	$0.120 \pm 0.016$	1.5	1.8–3.0	0.060	62	–35
ABELL 3739	1, 2	0.1651	$0.177 \pm 0.010$	1.3	1.6–2.1	0.054	63	–42
ABELL 3739	1, 6, 7	0.1786	$0.183 \pm 0.010$	1.3	1.6–2.1	0.054	63	–42
ABELL 3740	1, 3	0.1521	$0.141 \pm 0.007$	1.3	1.4–2.7	0.086	39	–42
ABELL 3836	1, 3	0.11	$0.120 \pm 0.007$	1.3	1.4–2.7	0.032	32	–51
RXC J2218.6–3853	8	0.1379	$0.138 \pm 0.022$	1.5	1.2–1.9	0.026	12	–56
ABELL 3866	1, 9	0.1544	$0.156 \pm 0.008$	1.4	1.1–1.9	0.020	22	–57
ABELL 3888	1, 10	0.152912	$0.159 \pm 0.016$	1.4	1.3–1.9	0.029	28	–59
AM 2250–633	9, 11	0.2112	$0.204 \pm 0.014$	1.2	1.1–1.4	0.046	26	–49

<sup>a</sup> References—(1) Abell et al. (1989), (2) Böhringer et al. (2004), (3) Struble & Rood (1999), (4) Katgert et al. (1996), (5) Zaritsky et al. (2006), (6) Voges et al. (1999), (7) Schwobe et al. (2000), (8) Cruddace et al. (2002), (9) de Grandi et al. (1999), (10) Pimblet et al. (2006), (11) Arp & Madore (1987).

<sup>b</sup> Spectroscopic redshift reported by references.

<sup>c</sup> Photometric redshift based on SLR color corrections, with standard errors on the mean redshift estimates of the brightest cluster member galaxies.

<sup>d</sup> Airmass at which the images were obtained.

<sup>e</sup> Range of seeing in the multiband images.

<sup>f</sup> SFD-predicted Galactic reddening in  $(g - i)$ .

<sup>g</sup> Number of stars used to determine the SLR color correction.

<sup>h</sup> Galactic latitude of the cluster.

as the standard error on the mean  $g - i$  color of the red sequence galaxies we selected, and cluster redshift errors were taken to be  $SE_{gi}/3$ , taken from the slope of the color-redshift relation of Lopes (2007). The reduced  $\chi^2$  of residuals is 0.6, so this error slightly overestimates the scatter. The residual cluster redshift RMS is  $\sigma_z = 0.007$ , or  $\sigma_z/(1+z) = 0.6\%$  for the range of redshifts we measured. We emphasize that this is the estimated redshift error not per red galaxy, but per cluster, each of which made use of an ensemble of red galaxies.

The  $\sigma_z = 0.007$  RMS error corresponds to  $g - i$  color errors of  $\sim 20$  mmag, again estimating from the roughly linear relationship between redshift and  $g - i$ . This level of residual error is roughly in accord with the SLR systematic errors due to Galactic dust and the atmosphere, estimated in §4.1, §4.2, and §4.3, and the residuals are inconsistent with erroneous Galactic dereddening. If Galactic extinction were completely unaccounted for by our calibration method, redshifts would lie along the dashed line of the right-hand panel of Figure 9, assuming no other systematic effects. Because our redshift residual trend is not consistent with the dashed line, these results provide further evidence (see §4.1) that SLR accounts for Galactic extinction in these fields.

## 5. DISCUSSION

We have provided a new way to calibrate instrumental photometry. It differs substantially from traditional techniques, and so a side-by-side comparison of SLR with traditional approaches is in order. This the first item of discussion. We then list in detail the unique advantages and limitations of SLR, and complete our discussion with tasks for the future.

### 5.1. SLR vs. Traditional Photometric Calibration

#### 5.1.1. Traditional Photometric Calibration

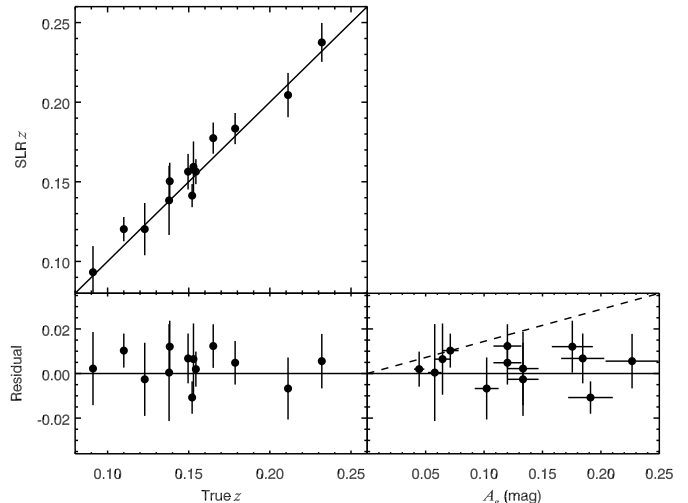


FIG. 9.— Photometric galaxy cluster redshifts from SLR-corrected colors vs. spectroscopic redshifts, and residuals. *Right panel*: Redshift residuals vs. expected  $g$ -band Galactic extinction. The red dashed line is the redshift error expected using colors that are not corrected for Galactic extinction. There is no evidence for a redshift residual correlated with Galactic extinction, indicating that SLR makes an appropriate correction.

The traditional path to calibrated colors has been to first calibrate magnitudes, then to subtract them. Magnitudes are calibrated by tying instrumental flux to photometric standard stars, which most often requires additional exposure time investment outside one’s field of scientific interest. The resulting zeropoints must be interpolated in space and time to the science fields, but only after extinction by the atmosphere is modeled and measured—which necessitates further standard field ob-

servations over a wide range of zenith angles.

The analysis of these data to extract calibrated colors traditionally involves the steps of:

1. Bias subtraction and flat-fielding;
2. Extracting instrumental magnitudes for all images, in all bands;
3. Using either observations of standard stars or program objects over a substantial span of zenith angles, in each band, to determine atmospheric extinction coefficients, and correcting each observation for atmospheric extinction;
4. Assessing whether the atmospheric conditions during observation were photometric, and thus whether the zeropoint and atmospheric extinction interpolations are valid;
5. Correcting for the frame-by-frame difference between PSF-fitting magnitudes and aperture photometry;
6. Determining and correcting for any differential sensitivity mismatch between the instrument and the desired photometric system, and applying these color term corrections to the photometry;
7. Determining Galactic extinction in the direction of the observation from some external source such as SFD, and making an appropriate correction to all magnitudes; and
8. Generating colors of sources of interest by subtracting these fully calibrated apparent magnitudes.

The result of this procedure is a source catalog that contains magnitudes and derived colors. Besides being costly in telescope time, this procedure is also suffers from extra uncertainty from the explicit mathematical modeling of atmospheric attenuation. Moreover, the individual magnitudes must each be calibrated to a better fractional precision than the desired color error. In the future, when high accuracy all-sky photometric catalogs of faint sources are readily available in all bands of interest, this process will be somewhat simplified. In the meantime we offer the SLR approach. SLR renders the preliminary magnitude calibration step unnecessary, instead allowing for the direct determination of colors of all objects of interest. SLR also provides a way to calibrate the photometry by tying the magnitude scale to the all-sky 2MASS catalog, again without the need for extra standard star observations.

#### 5.1.2. *SLR Photometric Calibration*

The SLR approach matches the distribution of stars in the instrumental color-color space to a standard stellar locus, allowing us to replace the traditional analysis path with a streamlined set of steps.

1. For each previously uncharacterized instrument, we observe only one field that contains stars whose calibrated magnitudes are known. This allows us to establish, in the traditional way, the instrumental color terms that arise from filter and detector differences.

2. All subsequent images are bias subtracted and flat-fielded.
3. Instrumental magnitudes are extracted for objects in each image.
4. Objects are immediately cast in instrumental color-color space, and we determine the transformations needed to bring the instrumental stellar locus into agreement with the universal, calibrated color properties of stars.
5. This color transformation is then applied to all photometry, producing calibrated colors for all measured objects.
6. If desired, calibrated photometric zeropoints are determined by bootstrapping the photometry to any stellar photometric catalog that overlaps the program fields. At the time of this writing, 2MASS is the obvious choice.

The result is a catalog of colors, and optionally magnitudes that are calibrated in a separate step and whose uncertainties do not factor into those of the colors. As a fundamentally different calibration technique, SLR has unique (in)sensitivities to astrophysical and instrumental effects. We break out the unique advantages and limitations these afford.

#### 5.2. *Advantages*

*SLR corrects for atmospheric extinction, even if time-variable.* — Atmospheric extinction distorts the apparent colors of celestial sources, compared to what would be observed at the top of the atmosphere. To first approximation, this produces a translation of stars in color-color space. The atmospheric transmission function is expected to change as a function of time, zenith angle, and azimuthal angle as parcels of aerosols and water vapor travel and evolve in the sky (cf Stubbs et al. 2007). Traditional airmass and zeropoint interpolations cannot account for this, unless specially designed systems to monitor atmospheric conditions along the line of sight are deployed in parallel during observation. Moreover, the  $\sim X^{1/2}$  airmass dependence of saturated water lines in the  $z$ -band is simply not modeled by most observers (§3.2). SLR is unique because it naturally corrects for all of these additive effects at once with  $\kappa$ , and is therefore insensitive to any additive mis-modeling of atmospheric extinction. We showed in §4.2 and §4.3 that SLR corrects for atmospheric attenuation in the  $z$ -band with sub-percent accuracy. Our SLR formalism also supports color-airmass corrections, but we have shown that we already achieve high quality atmospheric corrections through a wide range of airmasses without these.

*SLR corrects for attenuation through clouds.* — As long as the exposures are long enough to homogenize the extinction due to clouds blowing across the images being analyzed, then the SLR technique will compensate for a common flux diminution across each frame. Integration times that exceed 60 seconds typically satisfy this, even for images that span a degree on the sky. The multi-epoch SDSS Stripe 82 analysis of Ivezić et al. (2007) supports the assertion that we can treat the effect of clouds

as “grey” extinction, which SLR corrects for at once with  $\kappa$ .

*SLR corrects for passband sensitivity differences, even across different instruments and telescopes.* — An overall multiplicative difference between the system throughput vs. wavelength of two different cameras or telescopes can be caused by filter transmission functions, detector quantum efficiency, and other instrumental properties. These are some reasons the nominal zeropoints between two facilities are not equal. We have shown that SLR accounts for zeropoints in all tests we performed (§4). *Differential* variation in system throughput vs. wavelength brings about disagreements in apparent magnitudes and colors that change with objects’ color. The SLR technique takes these into account by applying traditional color terms, measured from infrequent standard star observations. In color-color space, these cause apparent colors to scale, shear, and rotate. Our SLR methodology fully permits color term correction, and we have demonstrated this in §4.2 and implicitly in §4.4 using two different cameras.

*SLR circumvents aperture corrections and photometric artifacts from PSF variations.* — Because the SLR technique maps observed, instrumental magnitudes onto a standard stellar locus, even if photometry from a given image in a given passband has some systematic photometry error from PSF-related issues, the applied color transformation will correct for these artifacts. Differences in aperture corrections between passbands produce a common displacement in color-color space. Ivezić et al. (2007) showed that using the stellar locus to correct colors of galaxies works well for photometry obtained with the SDSS analysis pipeline. We have demonstrated in §4.4 that applying SLR to Source Extractor instrumental magnitudes produces photometric redshifts that are in excellent agreement with spectroscopic redshifts, without additional aperture corrections.

*SLR avoids the need to take more than a single calibration frame per instrument, per filter.* — The universality of the stellar locus in effect allows the colors from a set of multiband images to be self-calibrating. We find that taking only one set of multiband images of a calibration field is required, to determine the instrumental color terms. At all times thereafter, on timescales of months or years, and as long as there is a sufficient number of stars ( $\gtrsim 10$ ) in each image being analyzed, there is no need to obtain additional calibration frames. Our galaxy cluster observations of §4.4 used color terms measured only once in an SDSS standard star field.

*SLR corrects for Galactic extinction, independent of  $A_V$  and  $R_V$ .* — Whatever processes might bring about an overall observed displacement of the stellar locus, SLR will make the appropriate correction as long as it is locally well correlated. This includes Galactic reddening effects when the stars are behind the dust. Because a single global color correction is applied to all the data, the cataloged objects should span a sufficiently small region on the sky to assure they have a common Galactic reddening. We showed in §4.1 that SLR can recover the canonical reddening through very high and very low dust thicknesses to  $\sim 20$  mag in color. We point out that our photometric redshift analysis in §4.4 made no explicit dust

correction of any kind, and results were nonetheless consistent with an intrinsic Galactic dereddening by SLR. The anomalous extinction results of §4.2 are suggestive of possible deviations from the typically assumed reddening law—although drifts in mean metallicity cannot be ruled out as yet.

*SLR takes advantage of all stars in the images, producing a “democratic” color calibration.* — For fields of view that are currently typical of astronomical imaging instruments, Galactic stars are approximately uniformly distributed across the image. SLR allows for the calibration of all objects in a field using the very stars appearing in that field. As long as there are no effects that vary across the field of view, the SLR color calibration technique inherently produces a homogenized calibration of colors across the frame.

*SLR uses a single common standard stellar locus, and thereby reduces sensitivity to systematic errors in photometric zeropoints.* — The photometry from SDSS exhibits sky point drifts at the few percent level across the sky (Padmanabhan et al. 2008). If these cataloged magnitudes are used to derive local colors, the colors inherit a position-dependent systematic drift that is the difference between the underlying photometric zeropoint errors. SLR uses a single common standard stellar locus for all color corrections, so the derived colors should show reduced position-dependent systematic errors. The *precision* of SLR-derived colors should be outstanding. The *accuracy* of SLR-derived colors depends upon the accuracy of the standard stellar locus, the extent to which this locus is representative of the population being observed, and the nature of the Galactic dust extinction, as discussed in §2.

*SLR is flexible.* — The simple matching of the observed instrumental stellar locus to a standard one allows for a diversity of input catalogs. The input can be purely flat-fielded, instrumental photometry, and SLR will correct them for atmospheric and Galactic extinction, and zeropoints. SLR will equally allow input photometry that has already been corrected for some or all of these effects, as previous authors have shown. We have applied SLR to pre-calibrated SDSS photometry (§4.2) and to instrumental photometry from two different instruments (§4.3, §4.4). The method makes no distinction between the various sources of locus shifts in color-color space, so it can be applied to photometric catalogs generated up to any stage in the traditional analysis chain. One can even envision mixing catalogs by, for example, acquiring *griz* imagery of a field and performing SLR, then acquiring further *z*-band images of the same field and coupling the new instrumental *z*-band catalogs to the already-calibrated *gri* ones. The resulting  $\kappa$  will produce the new *z*-band calibration, and should reproduce the *gri* calibrations. SLR can be optimized to give fast calibrations for a wide variety of optimized observing strategies. Of course, SLR will perform best when the prior reduction steps do not induce additional color scatter nor scalings, rotations, and shears.

*SLR is fast: mountaintop reductions can provide accurate colors, and hence photometric redshifts, on-the-fly.* — Optimizing the use of allocated telescope time is an important



goal. By performing real-time SLR reductions of photometric data, observers can determine when a desired signal to noise ratio is attained. A specific application of SLR by our group is the real-time determination of photometric redshifts of large numbers of galaxy clusters—an application we illustrated in §4.4. In upcoming runs we intend to use SLR to make adaptive adjustments of integration times while observing clusters of known position but unknown redshift.

### 5.3. Limitations

As a different way of calibrating photometry, SLR also carries some unique limitations. The main limitation is that SLR performs better in obtaining highly accurate colors than magnitudes in each of the bands. By the same token, the colors that are produced by the SLR approach are only as good as the standard stellar locus used as the calibration standard. Of particular concern is the need to identify a set of calibration stars that have suffered minimal Galactic extinction, and whose median metallicity reflects that of the stellar populations we observe in practice.

Another principal limitation is that SLR calibrations necessarily correct for Galactic extinction. To SLR, the dust correction is as natural as the atmospheric extinction correction. This is because our locus is standardized to stars suffering minimal extinction, while stars we observe in practice will almost always be behind the dust. It is, however, more common to calibrate photometry to the top of the atmosphere and only optionally apply an SFD Galactic extinction correction by hand, if needed. There is considerable uncertainty in our understanding of the dust, and this must be folded into our *a priori* color error estimates. In nearly all the fields we have studied, results suggest that SLR corrects extinction through a wide range of dust thicknesses with high accuracy. Users should take special care not to double-correct the extinction when using SLR.

Consequently, SLR will produce discrepant results if the sources of extinction vary significantly across the field of view. This introduces a trade-off between larger field size, which allows more stars to be included in the regression, and spatially constant extinction, which SLR corrects for best. We have applied SLR on small fields of view with as few as 7 useful stars, and the uncertainties in these cases are predominantly statistical. If SLR is to be applied to larger fields, one possible way to minimize extra scatter from Galactic extinction is to first apply the SFD dust correction for each stellar position, and then allow SLR to make the residual color calibration. For widely varying dust across a field, this should suppress the large scale gradients and thus unnecessary scatter in the stellar locus.

A third source of concern, both for traditional methods and SLR, are systematic differences between point source and galaxy photometry. Ivezić et al. (2007) and our own results demonstrate that applying a color correction derived from stars to galaxies does produce reliable photometric redshift estimates for red sequence galaxies. Some level of systematic error is nonetheless expected, because the spectral energy distributions (SEDs) of Galactic stars differ from the underlying SEDs of possibly redshifted galaxies of all types. Moreover, heavily extinguished sources with different intrinsic SEDs will not suffer identical color

shifts (McCall 2004). These are fundamental limitations of broadband photometry: as integrals over the product of a source’s SED, atmospheric and Galactic dust transmission functions, and the instrumental sensitivity curve, broadband measurements entangle the true SEDs with intervening attenuation effects almost irreversibly (Stubbs & Tonry 2006). This systematic error afflicts *all* photometry that uses stellar calibration standards, and is not unique to SLR.

We finally note that, in the optical, SLR implicitly requires the *g*-band. This is because the critical optical feature that makes our realization of SLR possible is the kink in the stellar locus at  $r-i \sim 0.7$ —the stellar locus in the  $(r-i, i-z)$  plane is virtually featureless. The kink (1) gives the one-dimensional locus line a distinctive shape that uniquely locates it in color-color space, and (2) provides a component of the locus that is nearly perpendicular to the reddening from Galactic and atmospheric extinction (see also Straizys et al. 1998). A purely linear stellar locus line does not allow for a *unique* stellar locus regression solution, as an instrumental locus could slide freely along that line. Inspection of Figure 1 reveals the importance of having *g*-band data.

### 5.4. Future Directions

*Standard locus refinements.*— We consider the standard stellar locus used for this paper to be a starting point. SLR’s performance rests on the standard locus being representative of the population that any given observation probes. It may be advantageous to develop different standard loci for different expected populations—for example, one for low Galactic latitudes, or different standard loci for different exposure times. The various standard loci could be measured empirically, or the expected perturbing effects could be modeled analytically and applied to the Covey et al. (2007) locus.

*A fuller treatment of Galactic extinction.*— As pointed out by McCall (2004), extinction by Galactic dust produces a shift in color that depends on the underlying photon spectral energy distribution of the source. For the current implementation of SLR we have ignored this effect, which will produce shears, scalings, and rotations as well as a simple translation in color-color space. These are analogous to color-airmass effects. We also expect that, if large fields must be calibrated in one SLR pass, it may be advantageous to apply the SFD correction for each stellar position first, as mentioned in §5.3. This may reduce scatter in stellar loci constructed from large data sets with widely varying extinctions.

*SLR vs. Galactic extinction and metallicity.*— This paper has shown that SLR accounts for the Galactic extinction in nearly all fields we have studied so far. The notable exceptions are the Stripe 82 results in §4.2, which corroborate those of Ivezić et al. (2007). Interestingly, the Galactic latitudes of the Stripe 82 fields where stellar locus methods fail are roughly equal to and *higher than* many of the fields we have used to recover the SFD extinction (§4.1) and measure cluster redshifts (§4.4). This presents difficulty in placing a hard lower bound on  $|b|$  where SLR should be valid. While we expect SLR to perform more reliably toward higher Galactic latitudes, we suspect SLR, by its nature, has the potential to make

*better* Galactic extinction corrections than SFD. This warrants extended and in-depth studies comparing SLR color shifts jointly to SFD prediction and metallicity.

*Other passband combinations.*— We have concentrated heavily on the *grizJ* bands, but the basic approach should be applicable to other photometric systems, such as *u*, *HK*, and *UBVRI*. MacDonald et al. (2004) have shown that the stellar locus as probed by the Johnson bands has a kink feature that makes this possible. We will also be interested to see how the PanSTARRS *y* band at  $1\ \mu\text{m}$  will add to the accuracy of SLR. Another interesting path to pursue is the use of the SLR approach to transform data between photometric systems.

*Multi-frame SLR.*— If we ignore color-airmass terms, then image stacks from individual frames taken at different airmasses should also be amenable to SLR analysis. A better approach, however, might be to extract SLR colors from all possible independent permutations of the multiband images, and then average the resulting colors. This is similar to the philosophy applied in the “ $N(N-1)$ ” approach to frame subtraction photometry for supernova cosmology (Barris et al. 2005), wherein all possible pairs of images are subtracted. This seems especially worth pursuing for multi-epoch surveys like PanSTARRS and LSST, as it completely sidesteps the challenges of combining frames with different PSFs obtained at different airmasses.

*Color recalibration of SDSS and 2MASS?*— If the stellar locus does in fact provide us with a uniform calibration source over most of the sky, and if SLR provides special insensitivities to anomalous atmospheric and Galactic extinction effects, then it is enticing to consider a joint recalibration of *colors only* from both the SDSS and 2MASS surveys. A Bayesian approach using the uniformity of the stellar locus, as was done in optical bands by Ivezić et al. (2007), might improve the accuracy of both optical and IR colors in these catalogs.

## 6. CONCLUSIONS

We have developed and demonstrated a technique that exploits the universality of the stellar locus to immediately obtain accurate colors from uncalibrated multiband data. For those who might wish to exploit the SLR approach, the core IDL tools we have developed are available at <http://stellar-locus-regression.googlecode.com>.

Using archived photometry from the SDSS survey, we have demonstrated that SLR can produce results that agree with the commonly used SFD extinction map over a wide range of dust thicknesses. The performance of SLR in these cases appears to be limited by systematic zeropoint drifts in SDSS magnitudes. We also reproduced the anomalous stellar locus reddening results of Ivezić et al. (2007) in a few SDSS Stripe 82 fields. This puts into question (1) the validity of the  $R_V = 3.1$  reddening law in those fields, (2) whether the dust is *both* in front of and behind the stars, and (3) whether these fields have stars with spatially correlated deviations from expected median metallicity.

Images of fields obtained through a wide range of airmasses were subjected to SLR analysis. We recovered the colors of the stars in these images with an uncertainty

limited by the Poisson and flat-field errors in the photometry from each frame. Using SLR-only techniques and 2MASS calibrated photometry, we additionally obtained *i*-band zeropoints in the fields good within 18 mmag.

Finally, we have also presented photometric redshift results using SLR-derived colors only. We recovered the spectroscopic redshifts of 11 galaxy clusters at redshifts  $0.09 < z < 0.25$  with  $\sigma_z/(1+z) = 0.6\%$  RMS residual error. The redshift residuals also showed that the red sequence galaxy colors from SLR alone were consistent with an intrinsic Galactic extinction correction.

The SLR technique, as implemented in our IDL code, can be used at the telescope in real-time to optimize the use of allocated telescope time. We regard SLR as a promising way to calibrate colors and magnitudes using fundamentally different physical assumptions, providing calibrations far faster than the traditional approach.

The approach outlined here builds upon the impressive work carried out in building and analyzing the SDSS and 2MASS data archives. We are grateful to the builders and operators of the SDSS and 2MASS systems. We also acknowledge our deep reliance on the groundwork laid by the authors of the Covey et al. (2007), Ivezić et al. (2008), Sesar et al. (2007), and Ivezić et al. (2007) papers. We are also grateful to the developers (Marigo et al. 2008) of the on-line stellar evolution modeling tool at <http://stev.oapd.inaf.it/cgi-bin/cmd2.1>. We are pleased to thank D. Finkbeiner, Z. Ivezić, T. Axelrod, A. Saha, D. Burke, J. Mohr, C. Smith, W. M. Wood-Vasey, A. Loehr, T. Stark, N. Suntzeff, J. Tonry, and J. Battat for valuable conversations.

This research has made use of the NASA/IPAC Extragalactic Database (NED) which is operated by the Jet Propulsion Laboratory, California Institute of Technology, under contract with the National Aeronautics and Space Administration. This publication has made use of data products from the Two Micron All Sky Survey, which is a joint project of the University of Massachusetts and the Infrared Processing and Analysis Center/California Institute of Technology, funded by the National Aeronautics and Space Administration and the National Science Foundation. This research has made use of the NASA/IPAC Infrared Science Archive, which is operated by the Jet Propulsion Laboratory, California Institute of Technology, under contract with the National Aeronautics and Space Administration.

Funding for the creation and distribution of the SDSS Archive has been provided by the Alfred P. Sloan Foundation, the Participating Institutions, the National Aeronautics and Space Administration, the National Science Foundation, the U.S. Department of Energy, the Japanese Monbukagakusho, and the Max Planck Society. The SDSS Web site is <http://www.sdss.org/>. The SDSS is managed by the Astrophysical Research Consortium (ARC) for the Participating Institutions. The Participating Institutions are The University of Chicago, Fermilab, the Institute for Advanced Study, the Japan Participation Group, The Johns Hopkins University, Los Alamos National Laboratory, the Max-Planck-Institute for Astronomy (MPIA), the Max-Planck-Institute for Astrophysics (MPA), New Mexico State University, Princeton

University, the United States Naval Observatory, and the University of Washington.

This work is supported by the NSF (AST-0607485), the DOE (DE-FG02-08ER41569), and Harvard Univer-

sity. We also thank the team of scientists, engineers and observing staff of the Las Campanas Observatory.

*Facilities:* Magellan:Baade (IMACS), Magellan:Clay (LDSS3), CTIO:2MASS, FLWO:2MASS, Sloan

## APPENDIX

### MOTIVATING THE COLOR TRANSFORMATION EQUATION

Equation (1) represents photometric calibrations using a compact, filter-independent matrix notation because in the future we wish our procedure to be applicable to any set of filters. In this appendix we give a concrete example for the *griz* SDSS filters in order to motivate and convey the meaning of the notation.

#### *Usual Photometric Calibration Equations*

Photometric calibrations are normally modeled with simple additive and sometimes multiplicative terms. Following the southern SDSS standards literature (Smith et al. 2002, 2003; Clem et al. 2007)<sup>11</sup> as rough guides, we relate the instrumental magnitude ( $g, r, i, z$ ) through the SDSS passbands to the true, extra-Galactic magnitude ( $g_0, r_0, i_0, z_0$ ) as

$$g = g_0 + a_g + E_g + A_g + b_g(g_0 - r_0) + c_g X_g(g_0 - r_0) \quad (\text{A1a})$$

$$r = r_0 + a_r + E_r + A_r + b_r(r_0 - i_0) + c_r X_r(r_0 - i_0) \quad (\text{A1b})$$

$$i = i_0 + a_i + E_i + A_i + b_i(i_0 - z_0) + c_i X_i(i_0 - z_0) \quad (\text{A1c})$$

$$z = z_0 + a_z + E_z + A_z + b_z(i_0 - z_0) + c_z X_z(i_0 - z_0) \quad (\text{A1d})$$

$$J = J_0, \quad (\text{A1e})$$

where in the last equality we take the 2MASS data to be calibrated already. Here,  $a_n$  is the zeropoint for the passband  $n$ ;  $E_n$  is the atmospheric extinction, often modeled as  $k_n X_n$  for some filter-dependent coefficient  $k_n$  and airmass  $X_n$  through which exposure  $R$  is taken; and  $A_n$  is the estimated Galactic extinction.  $b_n$  is the color coefficient, and  $c_n$  is the color-airmass cross term coefficient. The free parameters  $k_n$ ,  $a_n$ ,  $b_n$  and  $c_n$  can be estimated from the literature or measured using intermittent standard star observations, interpolating in airmass and in time to the science exposures. Galactic extinction is estimated using SFD.

#### *Corresponding Color Equations*

Colors are magnitude differences. Subtracting magnitudes between adjacent passbands using Equations (A1) gives

$$(g - r) = (g_0 - r_0) + (a_g - a_r) + (E_g - E_r) + (A_g - A_r) + \quad (\text{A2a})$$

$$b_g(g_0 - r_0) - b_r(r_0 - i_0) + c_g X_g(g_0 - r_0) - c_r X_r(r_0 - i_0) \quad (\text{A2b})$$

$$(r - i) = (r_0 - i_0) + (a_r - a_i) + (E_r - E_i) + (A_r - A_i) + \quad (\text{A2c})$$

$$b_r(r_0 - i_0) - b_i(i_0 - z_0) + c_r X_r(r_0 - i_0) - c_i X_i(i_0 - z_0) \quad (\text{A2d})$$

$$(i - z) = (i_0 - z_0) + (a_i - a_z) + (E_i - E_z) + (A_i - A_z) + \quad (\text{A2e})$$

$$b_i(i_0 - z_0) - b_z(i_0 - z_0) + c_i X_i(i_0 - z_0) - c_z X_z(i_0 - z_0) \quad (\text{A2f})$$

$$(z - J) = (z_0 - J_0) + a_z + E_z + A_z + \quad (\text{A2g})$$

$$b_z(i_0 - z_0) + c_z X_z(i_0 - z_0). \quad (\text{A2h})$$

This is greatly simplified with matrix notation. We define the instrumental color vector as

$$\mathbf{c} \equiv \begin{pmatrix} g - r \\ r - i \\ i - z \\ z - J \end{pmatrix}, \quad (\text{A3})$$

and likewise for the true color vector  $\mathbf{c}_0$ ; the additive color calibration vector as

$$\boldsymbol{\kappa} \equiv \begin{pmatrix} a_g - a_r + E_g - E_r + A_g - A_r \\ a_r - a_i + E_r - E_i + A_r - A_i \\ a_i - a_z + E_i - E_z + A_i - A_z \\ a_z + E_z + A_z \end{pmatrix}; \quad (\text{A4})$$

the color term matrix as

$$\mathbf{B} \equiv \begin{pmatrix} b_g & -b_r & 0 & 0 \\ 0 & b_r & -b_i & 0 \\ 0 & 0 & b_i - b_z & 0 \\ 0 & 0 & b_z & 0 \end{pmatrix}; \quad (\text{A5})$$

<sup>11</sup> For other relevant unpublished documents see [http://www-star.fnal.gov/Southern\\_griz/publications.html](http://www-star.fnal.gov/Southern_griz/publications.html)

and the color-airmass term matrix as

$$\mathbf{T} \equiv \begin{pmatrix} c_g X_g & -c_r X_r & 0 & 0 \\ 0 & c_r X_r & -c_i X_i & 0 \\ 0 & 0 & c_i X_i - c_z X_z & 0 \\ 0 & 0 & c_z X_z & 0 \end{pmatrix}; \quad (\text{A6})$$

then we can write the color calibration equations as a single matrix equation,

$$\mathbf{c} = \boldsymbol{\kappa} + (\mathbf{1} + \mathbf{B} + \mathbf{T}) \mathbf{c}_0, \quad (\text{A7})$$

where  $\mathbf{1}$  is the identity matrix. Setting  $\mathbf{T} = \mathbf{0}$ , this is equal to Equation (1). The inverse color transformation is

$$\mathbf{c}_0 = (\mathbf{1} + \mathbf{B} + \mathbf{T})^{-1} (\mathbf{c} - \boldsymbol{\kappa}). \quad (\text{A8})$$

Whether the transformation matrices are invertible depends on the details of how first order color coefficients are chosen, but under normal circumstances it will be possible. Using the example we've just presented,  $(\mathbf{1} + \mathbf{B})$  is invertible because its determinant is  $(1 + b_g + b_r + b_g b_r)(1 + b_i - b_z)$ , which is not equal to zero for typical (small) values of color terms.

This is how our matrix notation corresponds to typical photometric calibrations. The notation is trivially generalized to any filter set. The notation also motivates generalizations in choice of calibration parameters. For example, the color term matrix  $\mathbf{B}$  can be made to be diagonal, (anti-)symmetric, or populated entirely by different nonzero entries, depending only the particular application. Furthermore, higher order terms can be considered by including higher powers of  $\mathbf{c}_0$  to Equation (A7).

#### REFERENCES

- Abell, G. O., Corwin, Jr., H. G., & Olowin, R. P. 1989, *ApJS*, 70, 1
- Arp, H. C. & Madore, B. F. 1987, *A Catalogue of Southern Peculiar Galaxies and Associations 2 volume set (A Catalogue of Southern Peculiar Galaxies and Associations 2 volume set, by Halton C. Arp and Barry F. Madore, pp. 504. ISBN 0521343364. Cambridge, UK: Cambridge University Press, May 1987.)*
- Barris, B. J., Tonry, J. L., Novicki, M. C., & Wood-Vasey, W. M. 2005, *AJ*, 130, 2272
- Böhringer, H., Schuecker, P., Guzzo, L., Collins, C. A., Voges, W., Cruddace, R. G., Ortiz-Gil, A., Chincarini, G., De Grandi, S., Edge, A. C., MacGillivray, H. T., Neumann, D. M., Schindler, S., & Shaver, P. 2004, *A&A*, 425, 367
- Brott, I. & Hauschildt, P. H. 2005, in *ESA Special Publication*, Vol. 576, *The Three-Dimensional Universe with Gaia*, ed. C. Turon, K. S. O'Flaherty, & M. A. C. Perryman, 565–
- Clem, J. L., Vanden Berg, D. A., & Stetson, P. B. 2007, *AJ*, 134, 1890
- Covey, K. R., Ivezić, Ž., Schlegel, D., Finkbeiner, D., Padmanabhan, N., Lupton, R. H., Agüeros, M. A., Bochanski, J. J., Hawley, S. L., West, A. A., Seth, A., Kimball, A., Gogarten, S. M., Claire, M., Haggard, D., Kaib, N., Schneider, D. P., & Sesar, B. 2007, *AJ*, 134, 2398
- Cruddace, R., Voges, W., Böhringer, H., Collins, C. A., Romer, A. K., MacGillivray, H., Yentis, D., Schuecker, P., Ebeling, H., & De Grandi, S. 2002, *ApJS*, 140, 239
- de Grandi, S., Böhringer, H., Guzzo, L., Molendi, S., Chincarini, G., Collins, C., Cruddace, R., Neumann, D., Schindler, S., Schuecker, P., & Voges, W. 1999, *ApJ*, 514, 148
- Dressler, A. M., Sutin, B. M., & Bigelow, B. C. 2003, in *Society of Photo-Optical Instrumentation Engineers (SPIE) Conference Series*, Vol. 4834, *Society of Photo-Optical Instrumentation Engineers (SPIE) Conference Series*, ed. P. Guhathakurta, 255–263
- Efron, B. 1979, *The Annals of Statistics*, 7, 1
- Finlator, K., Ivezić, Ž., Fan, X., Strauss, M. A., Knapp, G. R., Lupton, R. H., Gunn, J. E., Rockosi, C. M., Anderson, J. E., Csabai, I., Hennessy, G. S., Hindsley, R. B., McKay, T. A., Nichol, R. C., Schneider, D. P., Smith, J. A., York, D. G., & the SDSS Collaboration. 2000, *AJ*, 120, 2615
- Hawley, S. L., Covey, K. R., Knapp, G. R., Golimowski, D. A., Fan, X., Anderson, S. F., Gunn, J. E., Harris, H. C., Ivezić, Ž., Long, G. M., Lupton, R. H., McGehee, P. M., Narayanan, V., Peng, E., Schlegel, D., Schneider, D. P., Spahn, E. Y., Strauss, M. A., Szkody, P., Tsvetanov, Z., Walkowicz, L. M., Brinkmann, J., Harvanek, M., Hennessy, G. S., Kleinman, S. J., Krzesinski, J., Long, D., Neilsen, E. H., Newman, P. R., Nitta, A., Snedden, S. A., & York, D. G. 2002, *AJ*, 123, 3409
- Ivezić, Ž., Sesar, B., Jurić, M., Bond, N., Dalcanton, J., Rockosi, C. M., Yanny, B., Newberg, H. J., Beers, T. C., Allende Prieto, C., Wilhelm, R., Lee, Y. S., Sivarani, T., Norris, J. E., Bailer-Jones, C. A. L., Re Fiorentin, P., Schlegel, D., Uomoto, A., Lupton, R. H., Knapp, G. R., Gunn, J. E., Covey, K. R., Smith, J. A., Miknaitis, G., Doi, M., Tanaka, M., Fukugita, M., Kent, S., Finkbeiner, D., Munn, J. A., Pier, J. R., Quinn, T., Hawley, S., Anderson, S., Kiuchi, F., Chen, A., Bushong, J., Sohi, H., Haggard, D., Kimball, A., Barentine, J., Brewington, H., Harvanek, M., Kleinman, S., Krzesinski, J., Long, D., Nitta, A., Snedden, S., Lee, B., Harris, H., Brinkmann, J., Schneider, D. P., & York, D. G. 2008, *ApJ*, 684, 287
- Ivezić, Ž., Smith, J. A., Miknaitis, G., Lin, H., Tucker, D., Lupton, R. H., Gunn, J. E., Knapp, G. R., Strauss, M. A., Sesar, B., Doi, M., Tanaka, M., Fukugita, M., Holtzman, J., Kent, S., Yanny, B., Schlegel, D., Finkbeiner, D., Padmanabhan, N., Rockosi, C. M., Jurić, M., Bond, N., Lee, B., Stoughton, C., Jester, S., Harris, H., Harding, P., Morrison, H., Brinkmann, J., Schneider, D. P., & York, D. 2007, *AJ*, 134, 973
- Jurić, M., Ivezić, Ž., Brooks, A., Lupton, R. H., Schlegel, D., Finkbeiner, D., Padmanabhan, N., Bond, N., Sesar, B., Rockosi, C. M., Knapp, G. R., Gunn, J. E., Sumi, T., Schneider, D. P., Barentine, J. C., Brewington, H. J., Brinkmann, J., Fukugita, M., Harvanek, M., Kleinman, S. J., Krzesinski, J., Long, D., Neilsen, Jr., E. H., Nitta, A., Snedden, S. A., & York, D. G. 2008, *ApJ*, 673, 864
- Katgert, P., Mazure, A., Perea, J., den Hartog, R., Moles, M., Le Fevre, O., Dubath, P., Focardi, P., Rhee, G., Jones, B., Escalera, E., Biviano, A., Gerbal, D., & Giuricin, G. 1996, *A&A*, 310, 8
- Kurucz, R. L. 1993, *VizieR Online Data Catalog*, 6039, 0
- Larson, K. A. & Whittet, D. C. B. 2005, *ApJ*, 623, 897
- Lenz, D. D., Newberg, J., Rosner, R., Richards, G. T., & Stoughton, C. 1998, *ApJS*, 119, 121
- Lopes, P. A. A. 2007, *MNRAS*, 380, 1608
- MacDonald, E. C., Allen, P., Dalton, G., Moustakas, L. A., Heymans, C., Edmondson, E., Blake, C., Clewley, L., Hammell, M. C., Olding, E., Miller, L., Rawlings, S., Wall, J., Wegner, G., & Wolf, C. 2004, *MNRAS*, 352, 1255

- Marigo, P., Girardi, L., Bressan, A., Groenewegen, M. A. T., Silva, L., & Granato, G. L. 2008, *A&A*, 482, 883
- Marshall, D. J., Robin, A. C., Reyl e, C., Schultheis, M., & Picaud, S. 2006, *A&A*, 453, 635
- McCall, M. L. 2004, *AJ*, 128, 2144
- Morgan, W. W., Keenan, P. C., & Kellman, E. 1943, *An atlas of stellar spectra, with an outline of spectral classification* (Chicago, Ill., The University of Chicago press [1943])
- Nelder, J. A. & Mead, R. 1965, *Computer Journal*, 7, 308
- Osip, D. J., Floyd, D., & Covarrubias, R. 2008, in *Society of Photo-Optical Instrumentation Engineers (SPIE) Conference Series*, Vol. 7014, *Society of Photo-Optical Instrumentation Engineers (SPIE) Conference Series*
- Padmanabhan, N., Schlegel, D. J., Finkbeiner, D. P., Barentine, J. C., Blanton, M. R., Brewington, H. J., Gunn, J. E., Harvanek, M., Hogg, D. W., Ivezi c,  ., Johnston, D., Kent, S. M., Kleinman, S. J., Knapp, G. R., Krzesinski, J., Long, D., Neilsen, Jr., E. H., Nitta, A., Loomis, C., Lupton, R. H., Roweis, S., Snedden, S. A., Strauss, M. A., & Tucker, D. L. 2008, *ApJ*, 674, 1217
- Pimblet, K. A., Smail, I., Edge, A. C., O'Hely, E., Couch, W. J., & Zabludoff, A. I. 2006, *MNRAS*, 366, 645
- Schlegel, D. J., Finkbeiner, D. P., & Davis, M. 1998, *ApJ*, 500, 525
- Schwoppe, A., Hasinger, G., Lehmann, I., Schwarz, R., Brunner, H., Neizvestny, S., Ugryumov, A., Balega, Y., Tr mper, J., & Voges, W. 2000, *Astronomische Nachrichten*, 321, 1
- Sesar, B., Ivezi c,  ., Lupton, R. H., Juri c, M., Gunn, J. E., Knapp, G. R., DeLee, N., Smith, J. A., Miknaitis, G., Lin, H., Tucker, D., Doi, M., Tanaka, M., Fukugita, M., Holtzman, J., Kent, S., Yanny, B., Schlegel, D., Finkbeiner, D., Padmanabhan, N., Rockosi, C. M., Bond, N., Lee, B., Stoughton, C., Jester, S., Harris, H., Harding, P., Brinkmann, J., Schneider, D. P., York, D., Richmond, M. W., & Vanden Berk, D. 2007, *AJ*, 134, 2236
- Smith, J. A., Tucker, D. L., Allam, S. S., & Rodgers, C. T. 2003, *AJ*, 126, 2037
- Smith, J. A., Tucker, D. L., Kent, S., Richmond, M. W., Fukugita, M., Ichikawa, T., Ichikawa, S.-i., Jorgensen, A. M., Uomoto, A., Gunn, J. E., Hamabe, M., Watanabe, M., Tolea, A., Henden, A., Annis, J., Pier, J. R., McKay, T. A., Brinkmann, J., Chen, B., Holtzman, J., Shimasaku, K., & York, D. G. 2002, *AJ*, 123, 2121
- Smol ci c, V., Ivezi c,  ., Knapp, G. R., Lupton, R. H., Pavlovski, K., Ilij c, S., Schlegel, D., Smith, J. A., McGehee, P. M., Silvestri, N. M., Hawley, S. L., Rockosi, C., Gunn, J. E., Strauss, M. A., Fan, X., Eisenstein, D., & Harris, H. 2004, *ApJ*, 615, L141
- Straizys, V., Lazauskaite, R., Liubertas, R., & Azusienis, A. 1998, *Baltic Astronomy*, 7, 605
- Struble, M. F. & Rood, H. J. 1999, *ApJS*, 125, 35
- Stubbs, C. W., High, F. W., George, M. R., DeRose, K. L., Blondin, S., Tonry, J. L., Chambers, K. C., Granett, B. R., Burke, D. L., & Smith, R. C. 2007, *PASP*, 119, 1163
- Stubbs, C. W. & Tonry, J. L. 2006, *ApJ*, 646, 1436
- Voges, W., Aschenbach, B., Boller, T., Br uning, H., Briel, U., Burkert, W., Dennerl, K., Englhauser, J., Gruber, R., Haberl, F., Hartner, G., Hasinger, G., K rster, M., Pfeffermann, E., Pietsch, W., Predehl, P., Rosso, C., Schmitt, J. H. M. M., Tr mper, J., & Zimmermann, H. U. 1999, *A&A*, 349, 389
- Zaritsky, D., Gonzalez, A. H., & Zabludoff, A. I. 2006, *ApJ*, 638, 725